

1 **The brown adipocyte protein CIDEA promotes lipid droplet**
2 **fusion via a phosphatidic acid-binding amphipathic helix**

3 David Barneda¹, Joan Planas-Iglesias², Maria L. Gaspar³, Dariush Mohammadyani⁴,
4 Sunil Prasannan², Dirk Dormann⁵, Gil-Soo Han⁵, Stephen A. Jesch³, George M.
5 Carman⁶, Valerian Kagan⁴, Malcolm G. Parker¹, Nicholas T. Ktistakis⁷, Judith Klein-
6 Seetharaman^{2,4}, Ann M. Dixon⁸, Susan A. Henry³, Mark Christian^{1,2*}.

7 ¹ Institute of Reproductive and Developmental Biology, Imperial College London, London W12 0NN,
8 UK

9 ² Warwick Medical School, University of Warwick, Coventry, CV4 7AL, UK.

10 ³ Department of Molecular Biology and Genetics, Cornell University, Ithaca, New York 14853, USA.

11 ⁴ Department of Bioengineering, University of Pittsburgh, Pittsburgh, Pennsylvania 15219, USA.

12 ⁵ Microscopy Facility, MRC Clinical Sciences Centre, Imperial College London, London W12 0NN, UK

13 ⁶ Department of Food Science, Rutgers Center for Lipid Research, Rutgers University, New Brunswick,
14 New Jersey 08901, USA.

15 ⁷ Signalling Programme, Babraham Institute, Cambridge CB22 3AT, UK.

16 ⁸ Department of Chemistry, University of Warwick, Coventry, CV4 7AL, UK.

17

18

19 *Corresponding author.

20 E-mail: m.christian@warwick.ac.uk

21 Phone number: 44 2476 96 8585

22

23 **Summary**

24 Maintenance of energy homeostasis depends on the highly regulated storage and
25 release of triacylglycerol primarily in adipose tissue and excessive storage is a feature of
26 common metabolic disorders. CIDEA is a lipid droplet (LD)-protein enriched in brown
27 adipocytes promoting the enlargement of LDs which are dynamic, ubiquitous organelles
28 specialized for storing neutral lipids. We demonstrate an essential role in this process
29 for an amphipathic helix in CIDEA, which facilitates embedding in the LD
30 phospholipid monolayer and binds phosphatidic acid (PA). LD pairs are docked by
31 CIDEA trans-complexes through contributions of the N-terminal domain and a C-
32 terminal dimerization region. These complexes, enriched at the LD-LD contact site,
33 interact with the cone-shaped phospholipid PA and likely increase phospholipid barrier
34 permeability, promoting LD fusion by transference of lipids. This physiological process
35 is essential in adipocyte differentiation as well as serving to facilitate the tight coupling
36 of lipolysis and lipogenesis in activated brown fat.

37

38 **Introduction**

39 Evolutionary pressures for survival in fluctuating environments that expose
40 organisms to times of both feast and famine have selected for the ability to efficiently
41 store and release energy in the form of triacylglycerol (TAG). However, excessive or
42 defective lipid storage is a key feature of common diseases such as diabetes,
43 atherosclerosis and the metabolic syndrome (1). The organelles that are essential for
44 storing and mobilizing intracellular fat are lipid droplets (LDs) (2). They constitute a
45 unique cellular structure where a core of neutral lipids is stabilized in the hydrophilic
46 cytosol by a phospholipid monolayer embedding LD-proteins. While most mammalian
47 cells present small LDs ($<1\ \mu\text{m}$) (3), white (unilocular) adipocytes contain a single giant
48 LD occupying most of their cell volume. In contrast, brown (multilocular) adipocytes
49 hold multiple LDs of lesser size, increasing the LD surface/volume ratio which
50 facilitates the rapid consumption of lipids for adaptive thermogenesis (4).

51 The exploration of new approaches for the treatment of metabolic disorders has
52 been stimulated by the rediscovery of active brown adipose tissue (BAT) in adult
53 humans (5, 6) and by the induction of multilocular brown-like cells in white adipose
54 tissue (WAT) (7). The multilocular morphology of brown adipocytes is a defining
55 characteristic of these cells along with expression of genes such as Ucp1. The
56 acquisition of a unilocular or multilocular phenotype is likely to be controlled by the
57 regulation of LD growth. Two related proteins, CIDEA and CIDEC promote LD
58 enlargement in adipocytes (8-10), with CIDEA being specifically found in BAT.
59 Together with CIDEB, they form the CIDE (cell death-inducing DFF45-like effector)
60 family of LD-proteins, which have emerged as important metabolic regulators (11).

61 Different mechanisms have been proposed for LD enlargement, including *in situ*
62 neutral lipid synthesis, lipid uptake and LD-LD coalescence (12-14). The study of CIDE
63 proteins has revealed a critical role in the LD fusion process in which a donor LD
64 progressively transfers its content to an acceptor LD until it is completely absorbed
65 (15). However, the underlying mechanism by which CIDEC and CIDEA facilitate the
66 interchange of triacylglycerol (TAG) molecules between LDs is not understood. In the
67 present study, we have obtained a detailed picture of the different steps driving this LD
68 enlargement process, which involves the stabilization of LD pairs, phospholipid
69 binding, and the permeabilization of the LD monolayer to allow the transference of
70 lipids.

71 **Results**

72 **CIDEA expression mimics the LD dynamics observed during the differentiation of**
73 **brown adipocytes.** To examine the processes controlling LD enlargement in brown
74 adipocytes we followed LD dynamics by time-lapse microscopy. During differentiation
75 of immortalized brown preadipocytes large LDs were formed by the fusion of pre-
76 existing LDs (Video 1). This fusion process was characterized by a slow and
77 progressive reduction in the volume of a donor LD until completely absorbed by an
78 acceptor LD (Figure 1A), which is characteristic of CIDE activity. As CIDEA is
79 selectively expressed in brown adipocytes and could have a prominent role in the
80 acquisition of their multilocular morphology, we explored the effects of its expression
81 in undifferentiated pre-adipocytes. After inducing CIDEA, LDs in pre-adipocytes
82 showed an equivalent dynamic pattern to that observed in differentiating brown cells,
83 with the progressive fusion of the initial LDs until a few large LDs remained in the cell
84 (Video 2). LD fusion was achieved by the slow transference of lipids between LDs, and
85 was preceded by the formation of small clusters of interacting LDs (Figure 1B). Given

86 the importance of this process in adipocyte dynamics, we decided to undertake a
87 comprehensive molecular analysis.

88 **Phases of CIDEA activity: LD targeting, LD-LD docking and LD growth.** The
89 ectopic expression of full length CIDEA induced the formation of large LDs through
90 LD fusion by lipid transfer (Figure 1C-D). Control cells lacking expression of CIDEA
91 did not show LD enlargement (Figure 1C). As many proteins are constructed of
92 domains, that are conserved across families and serve as their main structural and
93 functional units, we assessed the conserved regions within the CIDE proteins. By
94 comparing the 217 amino acid (aa) sequence of CIDEA with that of CIDEB and
95 CIDEA, 4 highly conserved regions can be identified (Figure 2A and Figure 2-Figure
96 Supplement 1). The N-terminal (N-term) domain of CIDEA is composed of a basic
97 region (2-72 aa) followed by an acidic sequence (73-110 aa). These distinctly
98 differently charged regions are indicated by protein crystallography studies to be
99 important for the dimerization of CIDE domain proteins (16-19). The CIDEA C-
100 terminal (C-term) is rich in basic aas and contains a highly conserved region (126-155
101 aa), and a basic and hydrophobic sequence (162-197 aa). Based on this sequence
102 analysis, we created an extensive collection of v5-tagged CIDE point and deletion
103 mutants to test their effects on LDs (Figure 2). Interestingly, certain mutations such as
104 R171E/R175E promoted the aggregation of the cellular LDs in a few “bunch of
105 grapes”-like LD clusters, but were unable to induce the transference of lipids between
106 them (Figure 2B). In other cases, as with the expression of CIDEA-(116-217)-v5, the
107 LDs remained small and dispersed throughout the cytoplasm despite the protein being
108 normally localized at their surface. Finally, some versions of CIDEA such as CIDEA-
109 (1-118)-v5 showed no LD localization and did not affect their size, number or
110 distribution. Together with the time-lapse results, this indicates that the molecular

111 mechanism of CIDEA is composed by three discrete phases: LD targeting, LD-LD
112 docking, and LD growth.

113 **A cationic amphipathic helix in C-term drives LD targeting.** All the CIDEA
114 constructs that showed impaired LD localization contained deletions or mutations in the
115 C-term hydrophobic and basic region (162-197 aa) (Figure 2C). In fact, the last 66 aas
116 of CIDEA were sufficient for LD localization, as shown with the expression of CIDEA-
117 (152-217)-v5, whereas it lacked the ability to facilitate the docking of LDs (Figure 2C
118 and 4A). Although it is known that the C-term domain of CIDE proteins is essential for
119 LD localization and enlargement (20, 21), only the structure of the N-term domain has
120 been solved (16-19). The CIDE-N domain (Pfam reference PF02017) has been
121 determined in members of the CIDE family (PDB Codes: 2eel (hCIDEA), 1D4B
122 (hCIDEB), 4MAC (mCIDEA), 4ikg (mCIDEA)), to aas 40-117, 34-100, and 41-118 in
123 hCIDEA, hCIDEB and mCIDEA, respectively. Thus, the sequence 163-180, which we
124 found essential for LD-targeting (Figure 2C), lacks direct structural information to date.
125 We therefore predicted its structure using *in silico* approaches. The region displayed
126 high probability of a helical conformation, with strongly amphipathic character (Figure
127 3A, 3B and Figure 3-Figure Supplement 1). To experimentally confirm the presence of
128 an amphipathic helix in the LD-targeting domain of CIDEA, Circular Dichroism (CD)
129 spectroscopy was used to estimate the secondary structure of a synthetic peptide
130 corresponding to residues 158-185 in CIDEA. The CD spectra in the presence of 0.1%
131 n-dodecyl- β -D-maltopyranoside confirmed the presence of α -helical structure (Figure
132 3C).

133 As some LD proteins are known to be bound to the LD membrane through
134 amphipathic helices (22, 23), we tested if this short sequence was sufficient for LD
135 targeting. While HA-(1-120)-CIDEA showed no LD localization and had no effect on

LD distribution or size, HA-CIDEA-(1-117)-(163-180) was partially localized on the LD surface and promoted LD clustering (Figure 3D). Furthermore, the deletion of this C-term sequence in CIDEA-Δ(163-179)-v5 completely eliminated LD localization in most of the cells (Figure 2B and Figure 2C), confirming its role in LD targeting. However, partial LD localization could be observed in a small percentage of cells, together with the presence of LD clusters. This was also observed in CIDEA-Δ(162-197)-v5 and was particularly frequent in CIDEA-(N172X)-v5, which contains a deletion in the middle of the helix. In contrast, no LD-targeting could be observed for the N-term fragment alone (1-118aa) (Figure 2C). This may indicate that other regions in C-term may contribute to LD localization, either by directly binding the LD membrane or by interacting with other LD proteins. Similarly, LD targeting was compromised when the amphipathic character of the helix was disrupted in CIDEA-(F166R/V169R/L170R)-v5 by introducing cationic aas in its hydrophobic face. Although LD localization was only lost in a small percentage of cells, in the remaining cells the LD staining was accompanied by a predominantly cytosolic localisation (Figure 3E and Figure 2C). In contrast, the predominant LD localization of wild type (wt) CIDEA was maintained in CIDEA-(K167E/R171E/R175E)-v5, which presents a charge inversion of the helix but maintains its amphipathic properties (Figure 3E and Figure 2C).

The amphipathic helix is essential for LD enlargement. In addition to its role in LD targeting, our data indicates that the cationic amphipathic helix in the C-term participates in the TAG transference step of CIDEA activity, as the charge inversion (K167E/R171E/R175E) did not affect LD targeting but completely blocked LD enlargement (Figure 2C). Despite not being essential for LD targeting, the cationic amino acids in the helix are highly conserved in vertebrates (Figure 3-Figure Supplement 3A). K167 is 100% conserved across all vertebrate species examined. R171

161 was conserved across vertebrates including birds, snakes, lizards, crocodiles, turtles,
162 marsupials, placental mammals, monotremes, although not in fish. R175 is also highly
163 conserved with only birds, dolphin and Nile Tilapia (a fish) lacking this residue.
164 Remarkably, an amphipathic helix is predicted in CIDEA of all the vertebrate species
165 examined (Figure 3-Figure Supplement 3B).

166 The absence of negative charges in the helix appeared as essential condition to
167 permit TAG transference, as a single inverted charge mutation such as R171E or R175E
168 was sufficient to block LD enlargement (Figure 2C). In contrast conservative
169 substitutions such as R171K or K167R did not affect CIDEA activity, and even the
170 substitution of the 3 basic aa to histidine in (K167H/R171H/R175H)-CIDEA-v5 was
171 compatible with the formation of large LDs, strongly supporting the conclusion from
172 sequence comparison that positive charges are required at these positions. As histidine
173 has a lower pKa value than arginine and lysine, it can carry a positive charge depending
174 on the pH and local environment which could explain the activity retained by this
175 protein.

176

177 **LD-LD docking is induced by the formation of CIDEA complexes.** Deletions in the
178 N-term domain of CIDEA impaired LD-LD docking, as shown by the increase in cells
179 displaying isolated LDs (Figure 2C). Furthermore, LD clustering could be induced by
180 forcing the LD localization of the N-term fragment through conjugation with the 18-aa
181 amphipathic helix (HA-CIDEA-(1-117)-(162-180)) (Figure 3C).

182 As the N-term of CIDEA forms a highly polarized structure prone to dimerize (16), we
183 hypothesized that LD-LD docking was induced by the N-term-N-term interaction of
184 CIDEA molecules in adjacent LDs (trans complexes). However, the C-term fragment
185 (116-217) retained some degree of LD-LD docking activity (Figure2C), indicating that

186 an additional interaction site could be present in this region. In fact, a complete blocking
187 of LD clustering was only observed with the shorter fragment 152-217, which lacks the
188 N-term and a section of the C-term (Figure 4A).

189 The formation of CIDEA-CIDEA complexes was confirmed by co-
190 immunoprecipitation (co-IP) of CIDEA-v5 with CIDEA-HA. Surprisingly, Co-IP was
191 observed with CIDEA-(116-217)-v5 but not CIDEA-(1-118)-v5, indicating that the C-
192 term was responsible for that interaction (Figure 4B). Interestingly, a similar percentage
193 of the input was co-IPed for constructs producing highly clustered LDs (CIDEA-
194 (R171E/R175E)-v5) and constructs showing few LD-LD contacts (CIDEA-v5 or
195 CIDEA-(116-217)-v5). Hence, this C-term interaction is largely independent of the
196 presence of LD-LD contacts, indicating that it may also occur in cis.

197 Within the C-term region, the deletion of the 162-197 sequence did not affect the
198 co-IP whereas the signal was largely reduced in CIDEA- Δ (126-155)-v5 (Figure 4B),
199 indicating that this conserved region was involved in the C-term interaction. However,
200 the residual interaction still detectable by co-IP could sustain the LD-docking activity,
201 as cells expressing this construct displayed normal LD clustering (Figure 4A and 4B).
202 CIDEA-(152-217)-v5 (Figure 4A and Figure 2), which showed no LD clustering and
203 lacks both the 126-155 interaction site and the N-term domain displayed a further
204 reduction on the co-IP signal (Figure 4B). Therefore, trans complexes through N-term
205 dimerization would be responsible for the LD clusters and weak co-IP signal observed
206 in CIDEA-(126-155)-v5. The lack of co-IP between the N-term fragment and the full
207 length CIDEA could be due to conformational and positional factors favouring the
208 interaction between the HA-tagged full length proteins in the LD or between the
209 cytosolic v5-tagged N-term fragments. In fact, co-IP between N-term fragments of
210 CIDEA was previously reported (18). This interaction could be disrupted with the point

211 mutations E87Q/D88N or R55E as predicted by the crystal structure of the N-term
212 fragment which reveals the formation of homodimers in which the positively charged
213 R46, R55 and R56 in one molecule interact with negative residues in the other (E87 and
214 D88) (18). Interestingly, we found the equivalent mutations in CIDEA (E79Q/D80N
215 and R47E) impaired LD docking, while R47Q and R47A, which would not create
216 repulsions between the interacting domains did not affect CIDEA activity (Figure 2C).
217 Taken together, these results suggest that both the C-term dimerization site (126-155)
218 and the N-term domain of CIDEA can contribute to LD-LD docking by forming
219 complexes with its counterparts on the adjacent LD.

220 **CIDEC differs from CIDEA in its dependence on the N-term domain.** The
221 differential expression of CIDEA and CIDEC in BAT and WAT could be related to the
222 acquisition of multilocular or unilocular morphologies in brown and white adipocytes
223 (24). While the ectopic expression of both CIDEA and CIDEC produce LD enlargement
224 in a similar manner, specific differences in their activity and regulation could achieve
225 discrete outcomes. In fact, whereas deletion of the N-term domain of CIDEA blocks LD
226 enlargement (Figure 2C), it has been described that the C-term fragment of CIDEC
227 retains its activity (15, 25). Here we show that similar to CIDEA, the N-term of CIDEC
228 is involved in LD-LD docking, as its deletion increases the fraction of cells displaying
229 isolated LDs (Figure 2C). However, in the cells where the C-term of CIDEC could
230 effectively induce LD-LD docking, large LDs were observed instead of LD clusters,
231 showing that although its docking efficiency is reduced, this region of CIDEC is
232 sufficient for docking and enlarging the LDs. This differs from CIDEA, in which the C-
233 term fragment cannot induce LD enlargement despite retaining a partial LD docking
234 activity. In addition to intrinsic differences between CIDEC and CIDEA, their activity
235 could be affected by the interaction with additional proteins. While PLIN1 interacts

with CIDEA, but not CIDEA, and potentiates its activity (18, 26) we have observed that CIDEA interacts with PLIN5 (Figure 4D), which is enriched in BAT (27, 28). In addition to PLIN5, CIDEA showed high affinity for both CIDEB and CIDEA, while it did not co-IP with DFF40 or DFF45, which share homology with the N-term domain of CIDE proteins (Figure 4C). As BAT cells express high levels of both CIDEA and CIDEA, the formation of CIDE heterocomplexes could be involved in the regulation of LD enlargement to retain the multilocular state.

CIDEA interacts with Phosphatidic Acid.

To further characterize the interaction of CIDEA with the LD membrane, we utilized lipid strips to investigate the affinity of CIDEA for different lipids present in mammalian cell membranes, finding that it selectively bound a set of anionic phospholipids (Figure 5A). The interaction with phosphatidic acid (PA) was of particular interest, as increased levels of this phospholipid have been linked with LD fusion (29) and the identification of enzymes such as AGPAT3 and LIPIN-1 γ in LDs supports the existence of *in situ* generation and consumption of PA (13, 30). PA binding was confirmed by the strong affinity of CIDEA-v5 for PA-beads (Figure 5B), which was greatly reduced by pre-incubation of the lysate with soluble PA, but not phosphatidylcholine (PC). Although the N-term fragment showed some residual affinity, the main PA-binding site of CIDEA was in the C-term region containing the amphipathic helix (163-180) (Figure 5C). The charge inversion of its 3 cationic amino acids resulted in the loss of affinity for PA-beads in the inactive mutant (K167E/R171E/R175E)-CIDEA-v5 without affecting its LD localization (Figure 5C), linking PA-binding with the TAG-transference step (Figure 5D).

To investigate if PA affects the structure of the amphipathic helix, we repeated the CD analyses in phosphate buffer in the presence and absence of DLPC lipid vesicles

261 with and without DLPA. Fitting of the CD data suggested a low (~5%) helical content
262 for the wild-type peptide when analysed in phosphate buffer alone, and indicated a
263 predominantly sheet / coil structure in the absence of detergent or liposomes. The
264 presence of DLPC liposomes stabilized a sharp increase in α -helical structure (up to
265 40%) and an equivalent reduction of sheet content (Figure 5E and Figure 5-Figure
266 Supplement 1), yielding higher helical content than that observed in n-dodecyl- β -D-
267 maltopyranoside micelles (~25%, Figure 3C). In contrast, the induction of helix
268 formation by DLPC was not observed in a mutant peptide carrying the substitutions
269 impairing LD-targeting in CIDEA-(F166R/V169R/L170R)-v5 (Figure 5E). This mutant
270 peptide remained predominantly random coil in the absence and presence of DLPC
271 liposomes. Interestingly, fitting of the CD data indicated significant helical content for
272 both the wt and mutant peptides in the presence of DLPC:DLPA (9:1) vesicles (Figure
273 5E and Figure 5-Figure Supplement 1). This indicates that the interaction with the
274 negatively charged phospholipid PA can compensate for the excess of positive charges
275 in CIDEA-(F166R/V169R/L170R)-v5.

276 To obtain more detailed insight into the interaction of the amphipathic helix with
277 phospholipids and the role of PA in this process, its interaction with LDs was modelled
278 by coarse-grained molecular dynamics (CG-MD) simulations (Figure 5F-H). CG-MD
279 simulations are well established for lipid containing systems (31), including LDs (32)
280 and have the advantage over full atomistic simulations that the time scales required are
281 much smaller allowing us to compare different LD compositions and helix mutants in
282 the large multimolecular LD system. The wt (163-180) helix
283 (CTSFKAVLRNLLRFMSYA) diffused toward the LD containing 400 palmitoyl-
284 oleoyl-glycero-phosphocholine (POPC) and 200 TAG molecules where it interacted at
285 its full length with the LD surface and penetrated into the hydrophobic region of the

286 phospholipid monolayer covering the TAG core (Figure 5F and 5G). A similar
287 behaviour was observed by the charge inverted mutant K167E/R171E/R175E (Figure
288 5G and Figure. 5-Figure Supplement 2), supporting the experimental result that these
289 mutations do not affect LD localization in CIDEA (Figure 2C and Figure 3E). In
290 contrast, no interaction with the LD was observed with the non-amphipathic
291 F166R/L169R/V169R (Figure 5G), which also impairs LD binding in CIDEA (Figure
292 2C and Figure 3E) and which was unable to attain stable secondary structure as
293 evidenced by CD (Figure 5E). Similarly, a non-amphipathic α -helix in N-term
294 (SSLQELISKTLVDLVITT) also showed no interaction with the LD (Figure 5G).

295 To study the effect of PA on LD structure and interaction with the CIDEA helix,
296 we replaced 10% of the PC molecules with PA. The equilibration of the system resulted
297 in a slight deformation of the spherical shape of the LD (Figure 5-Figure supplement 2).
298 The wt helix made a stable complex with this LD at even earlier simulation times than
299 with the PC-only containing LDs (Figure 5G and Figure 5-Figure Supplement 2). The
300 triple-E replacement mutant was also able to bind this LD, and even the
301 F166R/L169R/V169R mutant was now able to interact with the membrane (Figure 5G).
302 This result fits well with the CD results where the addition of PA also rescued the helix
303 induction in this mutant peptide through interaction with the liposomes (Figure 5E).
304 Interestingly, while the presence of PA permitted the accommodation of the
305 F166R/L169R/V169R helix in the LD monolayer, it could not penetrate as deep toward
306 the TAG core as the wt or helix. The average distance of the peptide to the centre of the
307 LD (\pm S.E.M.) was 5.6 ± 0.04 nm and 5.7 ± 0.03 nm for wt and K167E/R171E/R175E,
308 respectively. In the presence of PA the distance was 5.6 ± 0.02 nm, 5.7 ± 0.02 nm, and
309 6.1 ± 0.02 for wt, K167E/R171E/R175E and F166R/L169R/V169R, respectively (also

310 see Figure 5G and 5H). This result confirms that the presence of the hydrophobic face
311 was necessary for proper helix insertion in the LD monolayer.

312 The CD-MD simulations not only shed light on the interaction between the helix
313 and the LD, but also provided an indication of the mechanism by which this process
314 could lead to LD enlargement by TAG transference. We observed that TAG molecules
315 were able to escape the LD core and were integrated in the hydrophobic section of the
316 membrane (Figure 5H). This TAG infiltration was increased after the docking of the wt
317 helix in the membrane (Figure 5-Figure Supplement 3), suggesting that CIDEA could
318 promote the migration of TAG into the membrane as an intermediate state prior to the
319 transference to the acceptor LD. To complete the transference, the hydrophobic TAG
320 molecules should overcome the energy barrier constituted by the phospholipid polar
321 heads and water molecules in the LD-LD interface. Interestingly, we observed that the
322 wt helix could attract PA molecules in its vicinity by the interaction of its cationic
323 residues with the negatively charged polar head of PA (Figure 5H). A direct interaction
324 of the amphipathic helix with PA was also indicated by molecular docking using
325 Autodock Vina, which supported the role of the K167, R171 and R175 residues in the
326 interaction (Figure 5-Figure Supplement 4). Remarkably, CG-MD showed that whereas
327 the non-amphipathic cationic helix F166R/L169R/V169R also interacted with PA
328 molecules from its superficial docking position in the LD membrane, the anionic
329 amphipathic mutant K167E/R171E/R175E mutant was docked in a PA-depleted area
330 and avoided the PA molecules (Figure 5H). Although TAG infiltration was also
331 observed in this simulation and the helix was well embedded in the membrane, its
332 inability to attract PA molecules could be responsible for the lack of TAG transference
333 activity in CIDEA-(K167E/R171E/R175E)-v5 (Figure 5D). Taken together, these results
334 indicate that CIDEA binds the LD by embedding a cationic amphipathic helix into the

LD monolayer and that once there, it can interact with PA molecules, which could facilitate TAG transference.

We found that PA-binding was a feature common to all three members of the CIDE protein family (Figure 5C). Intriguingly, we determined that an inactive CIDE identified in a patient with lipodystrophy (33) contained a truncation (E186X), in the predicted PA-binding site. Although hCIDE-(E186X)-v5 and the equivalent mCIDEA-(N172X)-v5 were localized in LDs in a high percentage of cells, they were completely unable to induce LD enlargement (Figure 5I and Figure 2C). LD clustering activity and its ability to interact with CIDE proteins was not altered in hCIDE-(E186X)-v5 (Figure 5I and 5J), but it showed no affinity for PA (Figure 5K). Thus, PA-binding could be involved in the lipid transfer phase of CIDE activity.

PA is required for LD enlargement.

To confirm the requirement of PA binding, we examined the effect of PA depletion on CIDEA activity. While substantial alterations in the phospholipid composition of mammalian cells often compromise their viability, yeast cells offer a wide range of genetically modified strains with well characterized alterations in phospholipid metabolism (Figure 6A) (34). Thus, despite the absence of CIDE homologues in yeast (35), we explored the functionality of CIDEA in wild type and genetically modified strains of *S. cerevisiae* (Figure 6-source data 1).

Murine CIDEA could be stably expressed in yeast cells (Figure 6B), producing an increase in the size of their LDs (Figure 6C). Yeast cells expressing wt CIDEA, but not the inactive R171E/R175E mutant, contained fewer and larger LDs than the control (Figure 6D-F), indicating that murine CIDEA was functional in these cells. By measuring the frequency of supersized LDs (diameter above 0.5 μ m) and the total

number of LDs in strains with altered lipid metabolism we could determine in which yeast strains CIDEA was able to induce LD enlargement (Figure 6E-F). CIDEA was inactive in cells defective in phospholipase D (*pld1Δ*) (36), which catalyzes the production of PA from PC. CIDEA activity was also abrogated in cells expressing a hyperactive form of the PA phosphohydrolase (PAH1-7A) (37, 38). These results indicate that PA is necessary for CIDEA activity. In addition, we observed that total cellular PA levels were increased by CIDEA, an effect that was prevented by the expression of PAH1-7A (Figure 6G). As the PA synthesis rate was not affected (Figure 6H), CIDEA could be protecting a pool of PA from degradation.

The deletion of diacylglycerol kinase (*dgk1Δ*) (39), did not affect CIDEA activity. *DGK1* is important for the generation of phospholipids from TAG as cells exit from stasis (40), but its deletion has not been shown to have a great effect on PA levels under normal growth conditions. Regarding *PAH1*, its deletion produces dramatic cellular effects (41), including defective LD formation (42, 43). As this alteration in LDs can be compensated by the deletion of *DGK1*, we chose to use the *dgk1Δpah1Δ* strain, observing normal LD enlargement by CIDEA (Figure 6E-F). CIDEA was also able to further increase the LD size in the *cho2Δ* strain, which lacks the phosphatidylethanolamine (PE) methylation pathway for PC synthesis, and has been shown to present supersized LDs and high levels of PA and PE (29). The CIDEA-induced LD enlargement in yeast was not due to a mere coating effect protecting LDs against lipases, as it was functional in the *tgl3Δtgl4Δtgl5Δ* strain, which lacks lipase activity. As expected, CIDEA could not induce the appearance of LDs in *dga1Δlro1Δare1Δare2Δ* cells (Figure 6D), which are deficient in the enzymes required for TAG and steryl ester synthesis and contain no LDs (44).

383 To study the role of PA-dependent CIDEA action in mammalian cells without
384 compromising other PA-dependent cellular processes, we specifically degraded this
385 phospholipid in LDs by overexpressing a LD-localized isoform of PA
386 phosphohydrolase (LIPIN-1 γ) (30, 45). While CIDEA-HA displayed normal activity in
387 cells co-transfected with an empty vector, it was unable to promote LD enlargement in
388 cells expressing LIPIN-1 γ -v5 (Figure 6I-J). LIPIN-1 γ -v5 showed affinity for PA but it
389 did not coIP with CIDEA, indicating that its inhibitory effects were not due to a direct
390 interaction between these proteins (Figure 6K-L). Taken together, these results reveal
391 that the mechanism of action of CIDEA involves direct interaction with PA molecules
392 in the LD monolayer.

393 Discussion

394 The Cidea gene is highly expressed in BAT, induced in WAT following cold
395 exposure (46), and is widely used by researchers as a defining marker to discriminate
396 brown or brite adipocytes from white adipocytes (7, 28). As evidence indicated a key
397 role in the LD biology (47) we have characterized the mechanism by which CIDEA
398 promotes LD enlargement, which involves the targeting of LDs, the docking of LD
399 pairs and the transference of lipids between them. The lipid transfer step requires the
400 interaction of CIDEA and PA through a cationic amphipathic helix. Independently of
401 PA-binding, this helix is also responsible for anchoring CIDEA in the LD membrane.
402 Finally, we demonstrate that the docking of LD pairs is driven by the formation of
403 CIDEA complexes involving the N-term domain and a C-term interaction site.

404 CIDE proteins appeared during vertebrate evolution by the combination of an
405 ancestor N-term domain and a LD-binding C-term domain (35). In spite of this, the full
406 process of LD enlargement can be induced in yeast by the sole exogenous expression of

407 CIDEA, indicating that in contrast to SNARE-triggered vesicle fusion, LD fusion by
408 lipid transference does not require the coordination of multiple specific proteins (48).
409 Whereas vesicle fusion implicates an intricate restructuring of the phospholipid bilayers,
410 LD fusion is a spontaneous process that the cell has to prevent by tightly controlling
411 their phospholipid composition (23). However, although phospholipid-modifying
412 enzymes have been linked with the biogenesis of LDs (49, 50), the implication of
413 phospholipids in physiologic LD fusion processes has not been previously described.

414 Complete LD fusion by lipid transfer can last several hours, during which the
415 participating LDs remain in contact. Our results indicate that both the N-term domain
416 and a C-term dimerization site (aa 126-155) independently participate in the docking of
417 LD pairs by forming trans interactions (Figure 7). Certain mutations in the dimerization
418 sites that do not eliminate the interaction result in a decrease on the TAG transference
419 efficiency, reflected on the presence of small LDs docked to enlarged LDs. This
420 suggests that in addition to stabilizing the LD-LD interaction, the correct conformation
421 of the CIDEA complexes is necessary for optimal TAG transfer. Furthermore, the
422 formation of stable LD pairs is not sufficient to trigger LD fusion by lipid transfer. In
423 fact, although LDs can be tightly packed in cultured adipocytes, no TAG transference
424 across neighbour LDs is observed in the absence of CIDE proteins (15), showing that
425 the phospholipid monolayer acts as a barrier impermeable to TAG. Our CG-MD
426 simulations indicate that certain TAG molecules can escape the neutral lipid core of the
427 LD and be integrated within the aliphatic chains of the phospholipid monolayer. This
428 could be a transition state prior to the TAG transference and our data indicates that the
429 docking of the amphipathic helix in the LD membrane could facilitate this process.
430 However, the infiltrated TAGs in LD membranes in the presence of mutant helices, or

431 even in the absence of docking, suggests that this is not enough to complete the TAG
432 transference.

433 To be transferred to the adjacent LD, the TAGs integrated in the hydrophobic
434 region of the LD membrane should cross the energy barrier defined by the phospholipid
435 polar heads, and the interaction of CIDEA with PA could play a role in this process, as
436 suggested by the disruption of LD enlargement by the mutations preventing PA-binding
437 (K167E/R171E/R175E) and the inhibition of CIDEA after PA depletion. The minor
438 effects observed with more conservative substitutions in the helix, suggests that the
439 presence of positive charges is sufficient to induce TAG transference by attracting
440 anionic phospholipids present in the LD membrane. PA, which requirement is indicated
441 by our PA-depletion experiments, is a cone-shaped anionic phospholipid which could
442 locally destabilize the LD monolayer by favoring a negative membrane curvature
443 incompatible with the spherical LD morphology (51). Interestingly, while the zwitterion
444 PC, the main component of the monolayer, stabilizes the LD structure (23), the
445 negatively charged PA promote their coalescence (29). This is supported by our CD-
446 MD results which resulted in a deformation of the LD shape by the addition of PA. We
447 propose a model in which the C-term amphipathic helix positions itself in the LD
448 monolayer and interacts with PA molecules in its vicinity, which might include trans
449 interactions with PA in the adjacent LD. The interaction with PA disturbs the integrity
450 of the phospholipid barrier at the LD-LD interface, allowing the LD to LD transference
451 of TAG molecules integrated in the LD membrane (Figure 7). Additional alterations in
452 the LD composition could be facilitating TAG transference, as differentiating
453 adipocytes experience a reduction in saturated fatty acids in the LD phospholipids (52),
454 and in their PC/PE ratio (53) which could increase the permeability of the LD

455 membranes, and we previously observed that a change in the molecular structures of
456 TAG results in an altered migration pattern to the LD surface (32).

457 During LD fusion by lipid transfer, the pressure gradient experienced by LDs
458 favors TAG flux from small to large LDs (15). However, the implication of PA, a minor
459 component of the LD membrane, could represent a control mechanism, as it is plausible
460 that the cell could actively influence the TAG flux direction by differently regulating
461 the levels of PA in large and small LDs, which could be controlled by the activity of
462 enzymes such as AGPAT3 and LIPIN-1 γ (13, 30). This is a remarkable possibility, as a
463 switch in the favored TAG flux direction could promote the acquisition of a
464 multilocular phenotype and facilitate the browning of WAT (24). Interestingly, Cidea
465 mRNA is the LD protein-encoding transcript that experiences the greatest increase
466 during the cold-induced process by which multilocular BAT-like cells appear in WAT
467 (24). Furthermore, in BAT, cold exposure instigates a profound increase in CIDEA
468 protein levels that is independent of transcriptional regulation (54). The profound
469 increase in CIDEA is coincident with elevated lipolysis and de novo lipogenesis that
470 occurs in both brown and white adipose tissues after β -adrenergic receptor activation
471 (55). It is likely that CIDEA has a central role in coupling these processes to package
472 newly synthesized TAG in LDs for subsequent lipolysis and fatty acid oxidation.
473 Importantly, BAT displays high levels of glycerol kinase activity (56, 57) that facilitates
474 glycerol recycling rather than release into the blood stream, following induction of
475 lipolysis (58), which occurs in WAT. Hence, the reported elevated glycerol released
476 from cells depleted of CIDEA (28) is likely to be a result of decoupling lipolysis from
477 the ability to efficiently store the products of lipogenesis in LDs and therefore
478 producing a net increase in detected extracellular glycerol. This important role of
479 CIDEA is supported by the marked depletion of TAG in the BAT of Cidea null mice

480 following overnight exposure to 4 °C (28) and our findings that CIDEA-dependent LD
481 enlargement is maintained in a lipase negative yeast strain.

482 Cidea and the genes that are required to facilitate high rates of lipolysis and
483 lipogenesis are associated with the “browning” of white fat either following cold
484 exposure (46) or in genetic models such as RIP140 knockout WAT (59). The induction
485 of a brown-like phenotype in WAT has potential benefits in the treatment and
486 prevention of metabolic disorders (60). Differences in the activity and regulation of
487 CIDEC and CIDEA could also be responsible for the adoption of unilocular or
488 multilocular phenotypes. In addition to their differential interaction with PLIN1 and 5,
489 we have observed that CIDEC is more resilient to the deletion of the N-term than
490 CIDEA, indicating that it may be less sensitive to regulatory posttranslational
491 modifications of this domain. This robustness of CIDEC activity together with its
492 potentiation by PLIN1, could facilitate the continuity of the LD enlargement in white
493 adipocytes until the unilocular phenotype is achieved. In contrast, in brown adipocytes
494 expressing CIDEA the process would be stopped at the multilocular stage for example
495 due to post-translational modifications that modulate the function or stability of the
496 protein or alteration of the PA levels in LDs.

497 Further work will be required to characterize the physiological differences
498 between CIDEC and CIDEA and determine the influence of their interacting partners
499 and the role of proteins able to alter the LD PA levels, such as Lipin-1 γ . Abnormal
500 accumulation of large LDs have also been observed in non-adipocyte cells under other
501 pathological conditions such as liver steatosis and atherosclerosis (61). As enhanced
502 expression of CIDE proteins have been linked to these conditions (62-64), the
503 modulation of CIDE-triggered LD enlargement represents a potential therapeutic
504 strategy which requires the elucidation of its molecular mechanism.

505 In summary, we found that during LD fusion by lipid transference, CIDEA
506 ensures the close proximity of the LD membranes by forming trans complexes through
507 its N-term and its C-term dimerization sites. This protein complex will be anchored in
508 the LD-LD interface, forming the molecular environment necessary for TAG transport
509 across the membrane. Finally, the amphipathic helix embedded in the LD membrane,
510 interacts with the cone-shaped phospholipid PA, generating a local perturbation of the
511 monolayer integrity that would increase its permeability to TAG and enable its
512 exportation to the acceptor LD. The new mechanistic insight into the molecular events
513 underpinning LD dynamics revealed by this study highlight CIDEA and PA production
514 as targets for therapeutic modulation of LD accumulation.

515

516 **Acknowledgements**

517 We thank Dr. Carole Sztalryd for providing the Plin expression vectors, Dr. David
518 Savage for the hCIDEA constructs, and Prof Parmjit Jat for providing retrovirus to
519 express the temperature-sensitive SV40 large T antigen. We are also grateful to Dr.
520 Vishwajeet Puri for critical reading of the manuscript. This work was supported by the
521 BBSRC grant BB/H020233/1, the EU FP7 project DIABAT (HEALTH-F2-2011-
522 278373), the Genesis Research Trust and by National Institutes of Health grants GM-
523 19629 (to S.A.H.) and GM-28140 (to G.M.C.)

524

525 **Materials and Methods**

526 **Plasmids and antibodies.** The coding region of murine Cidea, Cideb, Cidec, Dff40 and
527 Dff45 were cloned into the vector pcDNA3.1D/V5-His-TOPO (Invitrogen) to obtain the
528 v5-tagged versions of the proteins (47). The human full length and truncated forms of
529 Cidec were subcloned into pcDNA3.1D/V5-His-TOPO from their GFP constructs (33)
530 and Lipin-1 γ -v5 was constructed from pGH321 (45). Mutations and deletions were
531 generated with the QuikChange Lightning Kit (Agilent). Tagged proteins were detected
532 by using antibodies against v5 (Invitrogen, R96025), HA (Sigma, H6908) or GFP
533 (Abcam, ab1218).

534 **Cell culture and transfection.** 3T3-L1 cells were maintained in Dulbecco's modified
535 Eagle's medium (DMEM) containing 4.5 g/l glucose and L-glutamine supplemented
536 with 10% newborn calf serum (NCS, Invitrogen) and penicillin/streptomycin at 37 °C
537 and 5% CO₂. Hela cells were cultured in similar conditions but with 10% FBS
538 (Invitrogen). Transfections were performed using Lipofectamine 2000 (Invitrogen).
539 Stable cell lines expressing CIDEA-v5 were generated by transfection of 3T3-L1 cells
540 with pcDNA3.1/Cidea-v5 followed by selection with G418 (Invitrogen). The imBAT
541 cell line was generated by the retroviral transduction of primary brown adipocytes with
542 SV40 large-T antigen tsA58 mutant and differentiated as previously described (47).

543 **4D live cell imaging.** Cells in gelatin-coated glass-bottom dishes were stained with 0.1-
544 0.5 μ g/ml BODIPY 493/503 in the appropriate culture medium with 20 mM HEPES in
545 the absence of serum. After 10 minutes at 37 °C, 10% FBS was restored and the dish
546 was equilibrated at 37 °C in a Leica SP5 confocal microscope. Time-lapse Z-stacks
547 were acquired every 2 minutes, and represented as their maximum projection. 3T3-L1
548 cells were analysed 6 hours after infection with an adenovirus vector expressing CIDEA
549 (47). For the imBAT differentiation experiments, preadipocytes were incubated for 48

550 hours with differentiation cocktail (47), and medium was changed to DMEM:F12 with
551 10% FBS, 1nM T3 and 170 nM insulin for 6 hours before staining.

552 **Immunofluorescence.** Cells on glass coverslips were fixed in 4% paraformaldehyde,
553 and permeabilized with blocking solution (BS: 0.5% BSA, 0.05% Saponin, 50 mM
554 NH₄Cl, in PBS). Cells were incubated overnight at 4 °C with primary antibodies diluted
555 in BS, and for 1 hour at room temperature with secondary antibodies (conjugated to
556 Alexa488 and Alexa555, Invitrogen). Cells were stained in PBS with 2 µg/ml BODIPY
557 493/503 or 1:200 dilution of LipidToxTM Deep Red for 15 minutes and mounted in
558 ProLong® Gold antifade reagent (all from Invitrogen). Images were acquired in a Leica
559 TCS SP5 microscope. For the phenotypic distribution of Hela cells expressing modified
560 CIDEA–v5 constructs, cells were treated with oleic acid 24 hours after transfection and
561 incubated for further 18 hours prior to fixation. Phenotype classification was performed
562 by visual analysis of randomized samples in a minimum of three independent
563 experiments for each construct (n > 50 cells)

564 **Liposome Preparation.** Liposomes were prepared by dissolving lipid (1,2-dilauroyl-
565 sn-glycero-3-phosphocholine (DLPC, 12:0 PC) or a mixture of DLPC and DLPA (1,2-
566 dilauroyl-sn-glycero-3-phosphate, 12:0 PA) at a 9:1 DLPC:DLPA molar ratio) (Echelon
567 Biosciences Inc., USA) in 3:1 chloroform:MeOH and drying under vacuum using rotary
568 evaporation. The resulting thin films were left to dry under vacuum overnight to remove
569 all residual solvent, reconstituted in 25 mM sodium phosphate buffer (pH 7.2) to a final
570 lipid concentration of 3.3 mg/mL, and subjected to 4 times freeze-thaw-sonicate cycles.
571 The vesicles were incubated at 37°C for 20 minutes prior to CD measurements.

572 **Circular dichroism.** CD experiments were undertaken with a synthetic wild type
573 (SYDIRCTSFKAVLRNLLRFMSYAAQMTG) CIDEA peptide (Pepmic Co, Ltd,
574 Suzhou, China) encompassing aas 158-185 solubilized at a concentration of 41µM

575 (based on absorbance at 280nm) in 50 mM Potassium phosphate, pH 6.2 plus 0.1% n-
576 dodecyl- β -D-maltopyranoside and analysed by circular dichroism (CD) in a JASCO J-
577 815 spectrometer.

578 Additional CD experiments with the same wt peptide and a mutant
579 (F166R/V169R/L170R) (SYDIRCTSRKARRRNLLRFMSYAAQMTG) were carried
580 out using a Jasco J-1500 spectropolarimeter (Jasco UK, Great Dunmow, UK) equipped
581 with a Peltier thermally controlled cuvette holder and 1 mm path-length quartz cuvettes
582 (Starna, Optiglass Ltd, Hainault, UK). Spectra were recorded between 190-300 nm with
583 a data pitch of 0.2 nm, a bandwidth of 2 nm, a scanning speed of 100 nm min⁻¹ and a
584 response time of 1 second. Peptides were solubilized in 25 mM sodium phosphate (pH
585 7.2) at concentrations of 70 μ M (wt) and 47 μ M (mutant). Peptide samples were
586 prepared in the absence and presence of DPLC and DLPC:DLPA (9:1 molar ratio)
587 vesicles and CD spectra were acquired at 37°C. Data shown were averaged from four
588 individual spectra after subtraction of the appropriate buffer/vesicle CD spectrum. All
589 CD data was analysed using the CDPro suite of programs. The output of the individual
590 programs CDSSTR and CONTINLL provided the estimated percentages of α -helix, β -
591 sheet, turn and unstructured regions, using the IB=4 database of 43 soluble proteins with
592 CD data from 190 to 250 nm.

593 **Structure Prediction and Molecular Docking.** Secondary structure propensity of full-
594 length CIDEA was predicted using DSSP (65). The amphipathic helix sequence
595 CTSFKAVLRNLLRFMSYA (163-180 aa) was submitted to the PEP-FOLD online de
596 novo peptide structure prediction server using default settings (66). Phosphatidic acid
597 (PA) was docked to the PEP-FOLD predicted structure using default settings in a single
598 simulation by AutoDock Vina53 (<http://vina.scripps.edu>) (67). Lipid and protein
599 structures were converted from pdb into pdbqt format using MGL Tools54. A grid box

600 was centred at coordinates 35.651, 35.471, 35.569 with 34Å units in x, y and z
601 directions to cover the entire helix. AutoDock Vina reports the 9 lowest energy
602 conformations, which were inspected using PyMOL software (www.pymol.org).
603 According to binding affinity and visual inspection, without RMSD clustering, the best-
604 fit model has been selected.

605 **Coarse Grained Molecular Dynamics (CG-MD) simulations.** Coarse grained (CG)
606 molecular dynamics (MD) simulations were used to predict the structure of a lipid
607 droplet (LD) and its putative interaction with the amphipathic helix using a 4 to 1 atom
608 mapping for both, lipids and protein (31, 68). A LD composed of a hydrophobic core
609 containing 200 glyceryl trioleate or triacylglycerol (TAG) molecules surrounded by a
610 phospholipid monolayer containing 400 palmitoyl-oleoyl-glycero-phosphocholine
611 (POPC) molecules previously reported was used as the starting configuration (32). A
612 second LD containing PA consisting of a hydrophobic core of 200 TAG molecules, and
613 a phospholipid monolayer with 364 POPC molecules and 36 palmitoyl-oleoyl-glycero-
614 phosphatidic acid (POPA) was compiled using the same procedure. A rectangular
615 simulation box including LD, amphipathic helix, water and ions was energy minimized
616 and pre-equilibrated. All MD runs were carried out for 200ns under NPT conditions.
617 The CG-MD simulation of the LD-helix interaction was carried out using the MARTINI
618 CG force field developed by Marrink et al. (version 2.0) (31). All simulations were
619 performed using the GROMACS simulation package version 4.6.5
620 (<http://www.gromacs.org/>). The system was weakly coupled to an external temperature
621 bath at 310 K (69). The pressure was weakly coupled to an external bath at 1 bar using
622 an isotropic pressure scheme (69). Visualization and analysis was performed using the
623 VMD v.1.9 visualization software (70). Distances and density maps were computed

624 using analysis tools (g_dist and g_densmap) in the GROMACS package
625 (<http://www.gromacs.org>) (71).

626 **Immunoprecipitation (IP).** Cells were lysed in 50 mM Tris (pH 8.0), 150 mM NaCl,
627 1% TRITON X-100 with protease inhibitor cocktail (Roche). Anti-HA antibody
628 (H6908; Sigma) or anti-V5 antibody (R96025; Invitrogen) was bound to Dynabeads
629 Protein G (Invitrogen) and incubated with the lysate to IP the tagged proteins following
630 manufacturer's instructions. Cell lysates or IP fractions in Laemmli buffer were
631 analysed by Western blot. Each co-IP experiment was performed at least in triplicate,
632 producing similar results in each experiment with a representative image presented.

633 **Lipid binding assays.** In vitro translated CIDEA-v5 was synthesized from
634 pcDNA3.1/Cidea-v5 using the TnT® Coupled Wheat Germ Extract System (Promega),
635 and verified by Western blot. The cell-free preparation of CIDEA-v5 was probed with
636 Membrane Lipid Strips™ (Echelon) following the manufacturer's instructions. Protein
637 affinity for PA was examined in pull-down assays using PA covalently linked to
638 agarose beads (PA-beads) (72). Cells were lysed in 50 mM Tris-HCl pH 8.0, 50 mM
639 KCl, 10 mM EDTA, 0.5% Nonidet P-40 and protease inhibitors. Lysates were sonicated
640 and centrifuged at 14000g prior to incubation with the PA beads as previously described
641 (72). Competition experiments with soluble phospholipids were performed by
642 supplementing the cell lysate with 1,2-dilauroyl-sn-glycero-3-phosphate 12:0 PC
643 (DLPA) or 1,2-dilauroyl-sn-glycero-3-phosphocholine (DLPC) (Echelon). Each PA-
644 binding experiment was performed at least in triplicate, producing similar results in
645 each experiment with a representative image presented.

646 **CIDEA expression in yeast.** The *S. cerevisiae* strains used in this study are listed in
647 Supplemental File 1. To express CIDEA in yeast, a codon-optimized version of the
648 mouse Cidea gene was generated by artificial gene synthesis (GeneOracle), and

649 subcloned into pRS316-CYC1p. Wild type BY4742 (73) and genetically modified yeast
650 strains were transformed with pRS316-CYC1p-Cidea and stable transformants were
651 selected in synthetic media minus uracil. Leucine selection was used for the expression
652 of PAH1-7A with pHC204 (37).

653 **Microscopy analysis of yeast lipid droplets and image processing.** Yeast cells in
654 synthetic media cultured overnight at 30 °C were diluted to OD₆₀₀=0.1 and allowed to
655 grow until mid-logarithmic phase (OD₆₀₀=0.5) before fixation with 4% formaldehyde
656 and LD staining with 2 µg/ml BODIPY 493/503. For the automatic quantification of
657 LDs, random microscopy images were acquired using a Delta Vision RT system
658 (Applied Precision). Maximum intensity and integrated intensity projections were
659 created from the deconvolved image stacks using ImageJ. A custom written CellProfiler
660 pipeline (74) automatically identified individual yeast cells and measured their number
661 and size of circle shaped LDs. Supersized LDs were defined as the LDs with a diameter
662 above 0.5 µm.

663 **Steady state and pulse labeling of phospholipids.** To measure the total levels of
664 phospholipids in yeast, cells were grown overnight in synthetic medium at 30 °C in the
665 presence of 20 µCi/mL [³²P]-orthophosphate. Cultures were then diluted to OD₆₀₀=0.1
666 maintaining the label and were allowed to grow until OD₆₀₀=0.5. To analyse *de novo*
667 synthesis of glycerophospholipids, cells were grown to OD₆₀₀=0.5 in synthetic medium
668 and incubated with 100 µCi/mL [32P]-for 20 min. Lipids were extracted and quantified
669 by two-dimensional chromatography, as described by Gaspar et al (75).

670

671 **FIGURE Legends**

672 **Figure 1. CIDEA promotes LD enlargement by transference of lipids.** (A) Live
673 imaging of the LD dynamics during the differentiation of a brown preadipocyte,
674 showing the characteristic CIDE-triggered LD enlargement, characterized by the
675 progressive transference of lipids from a donor to an acceptor LD until it is completely
676 absorbed. (B) Live imaging of the LD dynamics in an undifferentiated 3T3-L1 cell 6
677 hours after infection with adenoviral particles carrying the CIDEA gene. Red arrows
678 highlight the transient formation of irregularly shaped LD clusters, while yellow arrows
679 mark the fusion of two droplets by transference of lipids. (C) CIDEA-v5 expression in
680 Hela cells induces LD enlargement. An enrichment in CIDEA-v5 (red) can be observed
681 in the contact site between two LDs (green). (D) Detail of LD fusion by slow
682 transference of lipids in a 3T3-L1 cell stably expressing CIDEA-v5.

683 **Figure 2. Mapping the functional domains of CIDEA.** (A) Amino acid sequence of
684 murine CIDEA, highlighting the residues conserved in either CIDEB or CIDEA (grey
685 underline) or in both proteins (black underline). The substituted aa in mutant constructs
686 appear in red, and a positively charged sequence necessary for the TAG transfer step is
687 encircled in orange. Four highly conserved regions are defined and symbolized by
688 colour boxes in a linear representation of CIDEA-v5. The theoretical isoelectric point of
689 each fragment is indicated inside the boxes. (B) Representative images of the different
690 phenotypes observed in Hela cells overexpressing mutated forms of CIDEA-v5. 24
691 hours after transfection cells were treated with oleic acid and incubated for further 18
692 hours prior to fixation. Cells were classified into 6 major phenotypes. Cells expressing
693 fully-active forms of CIDEA had few and large LDs (Type I). In some mutants, the
694 large LDs remained attached to many small LDs, indicating that lipid transfer was
695 inefficient or inactive for some LDs (Type II). When CIDEA alterations blocked the

lipid transfer process, the LDs remained small and grouped in a few large clusters (Type III). If this was accompanied by inefficient LD-LD docking, the cells contained a number of small LD clusters combined with isolated LDs (Type IV). The CIDEA forms which could not stabilize LD-LD interactions displayed a phenotype similar to the mock transfected cells, with most of the LDs dispersed thorough the cytoplasm (Type V). Finally, some CIDEA constructs were unable to target the LDs, indicating an alteration of the LD-binding domain (Type VI). (C) Morphologic distribution of cells expressing each of the studied CIDE constructs. The phenotypic distribution was performed in a minimum of three independent experiments for every construct (n > 50 cells).

Figure 2 – Figure Supplement 1. Alignment of amino acid sequences of CIDEA, CIDEB and CIDEA. Clustal format alignment of murine CIDEA, CIDEB and CIDEA, performed using T-COFFEE (www.tcoffee.org). Amino acid sequences were obtained from <http://ensembl.org>. "*" means residues are identical in all sequences in the alignment, ":" means conserved substitutions have been observed, "." means that semi-conserved substitutions are observed. Four highly conserved regions are defined by colour boxes.

Figure 3. CIDEA targets the LD monolayer through a cationic amphipathic helix. (A) Secondary structure of CIDEA predicted by SWISS-MODEL server. (B) Helical wheel representation of the putative amphipathic α -helix (163–180) generated at <http://heliquest.ipmc.cnrs.fr/>. (C) Circular Dichroism spectra of a 28-aa peptide corresponding to the 158-185 sequence of CIDEA (200 μ M) solubilized in 50 mM Potassium phosphate, pH 6.2 plus 0.1% n-dodecyl- β -D-maltopyranoside. (D) A HeLa cell expressing HA-CIDEA-(1-120)-v5 (red) or HA-CIDEA-(1-117)-(163-180) (red),

720 showing the inclusion of aas 163-180 enhances LD localization and the ability to
721 promote LD docking. The phenotypic distribution was performed in a minimum of three
722 independent experiments for every construct (n > 50 cells). **(E)** A HeLa cell expressing
723 CIDEA-(F166R/V169R/L170R)-v5 (red) showing amino acid substitutions to
724 compromise amphipathicity of the helix disrupt LD targeting, and a HeLa cell expressing
725 CIDEA-(K167E/R171E/R175/E)-v5 (red), showing amino acid substitutions to invert
726 the charge of the helix but maintaining amphipathicity retains predominantly LD
727 localization.

728 **Figure 3-Figure supplement 1. Conservation of amino acids for CIDEA**
729 **amphipathic helix across vertebrate species.** A) Alignment of amino acid sequences
730 for CIDEA over a range of vertebrate species corresponding to the amphipathic α -helix
731 (aas 163–180 of murine). Amino acid sequences were obtained from <http://ensembl.org>
732 and initially aligned using WebPRANK at <http://ebi.ac.uk>. Sequences were then
733 grouped based on species phylogeny. (B) Helical wheel representation of the CIDEA
734 putative amphipathic α -helix for indicated species (corresponding to murine aas 163–
735 180) generated at <http://heliquest.ipmc.cnrs.fr/>.

736 **Figure 4. LD-LD docking and CIDEA interactions.** (A) A HeLa cell expressing
737 CIDEA-(152-217)-v5, showing normal recruitment to LDs, but no LD docking. A HeLa
738 cell expressing CIDEA- Δ (126-155)-v5, showing normal LD-LD docking but inefficient
739 LD enlargement as revealed by the presence of clusters of small and large LDs.
740 Representative images are shown of experiments performed in a minimum of three
741 independent experiments for every construct (n > 50 cells). **(B)** Co-IP assays between
742 CIDEA-HA and different CIDEA-v5 constructs. The observed CIDEA-CIDEA
743 interaction was driven by the C-term domain and required the presence of the 126-155

744 aa sequence. **(C-D)** Co-IP assays showing CIDEA interactions with CIDEB, CIDEA
745 and PLIN5. Each co-IP was performed at least in triplicate, producing similar results in
746 each experiment.

747 **Figure 5. CIDEA is a PA binding protein.** **(A)** Lipid strip assay showing the affinity
748 of CIDEA-v5 for certain anionic phospholipids. **(B)** Interaction of CIDEA-v5 with PA-
749 beads. Binding was reduced by pre-incubation of the lysate with soluble PA, but not PC.
750 **(C)** The affinity for PA-beads was highly reduced in CIDEA-v5 constructs with
751 alterations in its C-term hydrophobic and basic region (162-197). **(D)** CIDEA-
752 (K167E/R171E/R175E)-v5 localizes to LDs and induces their clustering but cannot
753 promote their enlargement by lipid transfer. Representative images are shown of
754 experiments performed in a minimum of three independent experiments for every
755 construct (n > 50 cells). **(H)** Circular Dichroism spectra of the synthetic wild type (wt)
756 or mutant (F166R/V169R/L170R) CIDEA peptides encompassing aas 158-185
757 solubilized in 25 mM sodium phosphate (pH 7.2) at concentrations of 70 μ M (wt) and
758 47 μ M (mutant). Peptide samples were prepared in the absence and presence of
759 increasing amounts of DPLC or DLPC:DLPA (9:1 molar ratio). **(F-H)** CG-MD
760 simulations of peptide interactions with LDs (PC: hydrophobic chains, transparent blue,
761 polar heads, opaque blue; TAG: hydrophobic chains, dark brown, glycerol chain, light
762 brown; PA: hydrophobic chains, transparent red, polar heads, opaque red; peptides:
763 yellow, with cationic aa in blue and anionic in red). **(F)** Selected time points of the wt
764 helix simulation with PC-LDs. At 124 the helix initiates the contact through its
765 hydrophobic face, being rapidly embedded in the phospholipid monolayer. TAG
766 molecules can abandon the neutral lipid core and are integrated in the hydrophobic
767 region of the phospholipid monolayer. **(G)** Distance between the peptide and LD centre
768 of mass (COM) vs time for the different helices with a PC-LD and a PC:PA-LD. The

769 dashed line represents the approximate location of LD phospholipid head groups. **(H)**
770 Different views of the configuration of the LD-helix at the end of the simulations.
771 Interaction between the polar head of PA and the helix can be observed for the wt and
772 F166R/V169R/L170R but not K167E/R171E/R175E. **(I-K)** Comparison of full length
773 hCIDEA-v5 and the lipodystrophy-associated truncation hCIDEA-(E186X)-v5,
774 including LD localization and morphology **(I)**, co-IP with CIDEA-HA **(J)** and affinity
775 for PA-beads **(K)**. Each co-IP, PA-binding assay and Lipid strip assay was performed at
776 least in triplicate, producing similar results in each experiment.

777 **Figure 5-Figure Supplement 1. Secondary structure determination of CIDEA**
778 **amino acids 158-185 (wild type and F166R/V169R/L170R) by CDPro DATABASE**
779 **4 (43 soluble proteins) using the CONTINLL program.**

780

781 **Figure 5-Figure Supplement 2. Computational prediction of the amphipathic helix**
782 **and LD interactions. (A)** CG-MD simulations of peptide interactions with LDs (PC:
783 hydrophobic chains, transparent blue, polar heads, opaque blue; TAG: hydrophobic
784 chains, dark brown, glycerol chain, light brown; PA: hydrophobic chains, transparent
785 red, polar heads, opaque red; peptides: yellow, with cationic aa in blue and anionic in
786 red). Selected time points of the wt helix and K167E/R171E/R175E helix simulation
787 with PC-LDs or PC:PA-LDs are indicated.

788 **Figure 5-Figure Supplement 3. TAG infiltration into the phospholipid monolayer.**
789 **(A)** 2D number density maps of TAG molecules along the z direction from the CG-MD
790 simulations. TAG frequency was measured over 76 ns before and after the docking of
791 the wt helix to the membrane. The differential distribution before and after docking

792 reveals an increase on the presence of TAG molecules in the membrane, revealed by the
793 red spots in the outer arch and blue in the inner.

794 **(B)** CG-MD simulations of peptide interactions with LDs (PC: hydrophobic chains,
795 transparent blue, polar heads, opaque blue; TAG: hydrophobic chains, dark brown,
796 glycerol chain, light brown; PA: hydrophobic chains, transparent red, polar heads,
797 opaque red; peptides: yellow, with cationic aa in blue and anionic in red). Selected time
798 points of the wt helix with PC-LD show TAG molecules in the LD membrane were
799 increased after CIDEA peptide docking (170ns vs 24ns).

800 **Figure 5-Supplemental figure 4. Computational prediction of PA docking to the**
801 **amphipathic helix structure of CIDEA.** (A) Charge-smoothed potential of the
802 predicted putative amphipathic helix of murine CIDEA (aas 163-180). Stick
803 representation has been employed to highlight the positively charged residues K167,
804 R171 and R175. (B) The nine top-ranked models from molecular docking of PA and the
805 amphipathic helix using Autodock Vina. Interaction of the PA phosphate group with
806 R171 and R175 is observed in eight of them, while the hydrophobic chains of the
807 phospholipid can adopt multiple configurations.

808 **Figure 6. CIDEA is functional in yeast and requires PA.** (A) Pathway showing the
809 reactions catalyzed by the enzymes altered in the studied yeast strains. (B) Stable
810 expression of mCIDEA-v5 in three transformed yeast clones. (C) Frequency
811 distribution of the diameter of the largest LD per cell. (D) LD staining in the studied
812 yeast strains transformed with pRS316-CYC1p-Cidea or the empty vector. (E-F)
813 Quantification of LD size and number per cell in randomly acquired images (100-200
814 cells/condition). CIDEA activity in yeast was measured by its ability to increase the
815 percentage of cells with supersized LDs (E) and reduce the total number of LDs per cell

816 (F). (G-H) Effect of CIDEA and *PAH1-7A* expression in the cellular levels of PA (G)
817 and its synthesis rate (H). Three different yeast clones per condition were analysed, and
818 results are shown as the mean \pm s.e.m. One-way ANOVA with Bonferroni post-test was
819 performed to determine significant differences due to the presence of CIDEA (* P
820 <0.05 ; *** $P <0.001$). (I-L) Coexpression of hLIPIN-1 γ -v5 and CIDEA-HA in Hela
821 cells. (I) Representative immunofluorescence images showing LD staining (blue) in
822 Hela cells expressing CIDEA-HA (green) in the presence or absence of hLIPIN-1 γ -v5
823 (red). 24 hours after overexpression of hLIPIN-1 γ -v5 cells were transfected with
824 pcDNA3.1/Cidea-HA and incubated for further 24 hours. (J) Phenotypic distribution in
825 randomly selected cells ($n > 50$) showing the average values for three independent
826 experiments. (K) Co-IP assay in lysates of transfected Hela cells. (L) PA-beads binding
827 assay for hLIPIN-1 γ -v5. Each co-IP and PA-binding assay was performed at least in
828 triplicate, producing similar results in each experiment.

829 **Figure 6-source data 1.** List of yeast strains used in this study.

830 **Figure 7. Proposed molecular mechanism.** (A) CIDEA targets the LD through its C-
831 term amphipathic helix and once diffused to the LD surface, it forms cis CIDEA
832 complexes by interacting through the C-term (126-155) region. When two CIDEA-
833 containing LDs make contact, trans interactions between CIDEA molecules in each
834 droplet can be established, which will facilitate the docking of the LDs. Both the N-term
835 and the C-term would contribute by dimerizing with their counterparts of the neighbour
836 LD. This trans interaction will anchor the CIDEA complexes in the LD-LD contact site,
837 promoting a local enrichment of CIDEA. The monolayers of the two LDs will be
838 maintained at short distance by the CIDEA complex. The amphipathic helices,
839 embedded in the hydrophobic region of the membrane, will interact with the cone-

840 shaped PA, creating a local perturbation in the phospholipid barrier that will increase its
841 permeability to TAG. **(B)** The docking of the amphipathic helix to the membrane could
842 facilitate the integration of TAG molecules within the phospholipid hydrophobic tails.
843 Although the helix will be stabilized with its cationic residues pointing outwards, it will
844 interact with PA molecules in its vicinity, which could be pulled out of the monolayer
845 by the helix molecular dynamics. This could create a transitory discontinuity in the
846 polar barrier that will reduce the energy required to transfer the TAG molecules present
847 in the membrane. This alteration, together with the microenvironment created by the
848 CIDEA complex, will reduce the energy barrier necessary to transfer TAG molecules
849 between LDs, allowing the LD growth by lipid transference.

850 **Video 1. Lipid droplet enlargement in differentiating imBAT cells.** Immortalized
851 brown preadipocytes were induced to differentiate by incubation for 48 + 6 hours with
852 the described differentiation cocktails. The cell displays the characteristic LD
853 enlargement pattern triggered by CIDE proteins, defined by the progressive fusion by
854 lipid transference of the pre-existing LDs.

855 **Video 2. Lipid droplet enlargement induced by CIDEA.** LD dynamics in
856 undifferentiated 3T3-L1 cells 6 hours after infection with adenoviral particles carrying
857 the mouse Cidea gene. After CIDEA induction, the initial individual LDs form stable
858 contacts, reflected by small irregularly-shaped clusters of LDs. These interacting LDs
859 undergo an enlargement process by lipid transference, characterized by the progressive
860 enlargement of the acceptor LD and shrinkage of the donor LD until only a few large
861 LDs remain in the cell.

862

863 **References**

- 864 1. Greenberg AS, Coleman RA, Kraemer FB, McManaman JL, Obin MS, Puri V, et al. The
865 role of lipid droplets in metabolic disease in rodents and humans. *J Clin Invest.*
866 2011;121(6):2102-10.
- 867 2. Walther TC, Farese RV, Jr. Lipid droplets and cellular lipid metabolism. *Annu Rev*
868 *Biochem.* 2012;81:687-714.
- 869 3. Suzuki M, Shinohara Y, Ohsaki Y, Fujimoto T. Lipid droplets: size matters. *J Electron*
870 *Microsc (Tokyo).* 2011;60 Suppl 1:S101-16.
- 871 4. Cinti S. The adipose organ at a glance. *Dis Model Mech.* 2012;5(5):588-94.
- 872 5. Virtanen KA, Lidell ME, Orava J, Heglind M, Westergren R, Niemi T, et al. Functional
873 brown adipose tissue in healthy adults. *N Engl J Med.* 2009;360(15):1518-25.
- 874 6. Cypess AM, Kahn CR. Brown fat as a therapy for obesity and diabetes. *Curr Opin*
875 *Endocrinol Diabetes Obes.* 2010;17(2):143-9.
- 876 7. Harms M, P. S. Brown and beige fat: development, function and therapeutic potential.
877 *Nat Med.* 2013(10):1252-63.
- 878 8. Wu L, Zhou L, Chen C, Gong J, Xu L, Ye J, et al. Cidea controls lipid droplet fusion and
879 lipid storage in brown and white adipose tissue. *Science China Life sciences.* 2014;57(1):107-
880 16.
- 881 9. Puri V, Konda S, Ranjit S, Aouadi M, Chawla A, Chouinard M, et al. Fat-specific protein
882 27, a novel lipid droplet protein that enhances triglyceride storage. *J Biol Chem.*
883 2007;282(47):34213-8.
- 884 10. Puri V, Ranjit S, Konda S, Nicoloso SM, Straubhaar J, Chawla A, et al. Cidea is associated
885 with lipid droplets and insulin sensitivity in humans. *Proc Natl Acad Sci U S A.*
886 2008;105(22):7833-8.
- 887 11. Xu L, Zhou L, Li P. CIDE proteins and lipid metabolism. *Arterioscler Thromb Vasc Biol.*
888 2012;32(5):1094-8.
- 889 12. Kuerschner L, Moessinger C, Thiele C. Imaging of lipid biosynthesis: how a neutral lipid
890 enters lipid droplets. *Traffic.* 2008;9(3):338-52.
- 891 13. Wilfling F, Wang H, Haas JT, Krahmer N, Gould TJ, Uchida A, et al. Triacylglycerol
892 synthesis enzymes mediate lipid droplet growth by relocalizing from the ER to lipid droplets.
893 *Dev Cell.* 2013;24(4):384-99.
- 894 14. Bostrom P, Andersson L, Rutberg M, Perman J, Lidberg U, Johansson BR, et al. SNARE
895 proteins mediate fusion between cytosolic lipid droplets and are implicated in insulin
896 sensitivity. *Nat Cell Biol.* 2007;9(11):1286-93.
- 897 15. Gong J, Sun Z, Wu L, Xu W, Schieber N, Xu D, et al. Fsp27 promotes lipid droplet growth
898 by lipid exchange and transfer at lipid droplet contact sites. *J Cell Biol.* 2011;195(6):953-63.
- 899 16. Lugovskoy AA, Zhou P, Chou JJ, McCarty JS, Li P, Wagner G. Solution structure of the
900 CIDE-N domain of CIDE-B and a model for CIDE-N/CIDE-N interactions in the DNA
901 fragmentation pathway of apoptosis. *Cell.* 1999;99(7):747-55.
- 902 17. Wang X, Zhang B, Xu D, Gao J, Wang L, Wang Z, et al. Purification, crystallization and
903 preliminary X-ray crystallographic analysis of the CIDE-N domain of Fsp27. *Acta Crystallogr Sect*
904 *F Struct Biol Cryst Commun.* 2012;68(Pt 12):1529-33.
- 905 18. Sun Z, Gong J, Wu H, Xu W, Wu L, Xu D, et al. Perilipin1 promotes unilocular lipid
906 droplet formation through the activation of Fsp27 in adipocytes. *Nat Commun.* 2013;4:1594.
- 907 19. Lee SM, Jang TH, Park HH. Molecular basis for homo-dimerization of the CIDE domain
908 revealed by the crystal structure of the CIDE-N domain of FSP27. *Biochemical and biophysical*
909 *research communications.* 2013;439(4):564-9.
- 910 20. Liu K, Zhou S, Kim JY, Tillison K, Majors D, Rearick D, et al. Functional analysis of FSP27
911 protein regions for lipid droplet localization, caspase-dependent apoptosis, and dimerization
912 with CIDEA. *Am J Physiol Endocrinol Metab.* 2009;297(6):1395-413.

- 913 21. Christianson JL, Boutet E, Puri V, Chawla A, Czech MP. Identification of the lipid droplet
914 targeting domain of the Cidea protein. *Journal of lipid research*. 2010;51(12):3455-62.
- 915 22. Hinson ER, Cresswell P. The antiviral protein, viperin, localizes to lipid droplets via its N-
916 terminal amphipathic alpha-helix. *Proc Natl Acad Sci U S A*. 2009;106(48):20452-7.
- 917 23. Krahmer N, Guo Y, Wilfling F, Hilger M, Lingrell S, Heger K, et al. Phosphatidylcholine
918 synthesis for lipid droplet expansion is mediated by localized activation of CTP:phosphocholine
919 cytidylyltransferase. *Cell Metab*. 2011;14(4):504-15.
- 920 24. Barneda D, Frontini A, Cinti S, Christian M. Dynamic changes in lipid droplet-associated
921 proteins in the "browning" of white adipose tissues. *Biochim Biophys Acta*. 2013;1831(5):924-
922 33.
- 923 25. Jambunathan S, Yin J, Khan W, Tamori Y, Puri V. FSP27 promotes lipid droplet
924 clustering and then fusion to regulate triglyceride accumulation. *PLoS One*. 2011;6(12):e28614.
- 925 26. Grahn TH, Zhang Y, Lee MJ, Sommer AG, Mostoslavsky G, Fried SK, et al. FSP27 and
926 PLIN1 interaction promotes the formation of large lipid droplets in human adipocytes.
927 *Biochemical and biophysical research communications*. 2013;432(2):296-301.
- 928 27. Harms M, Seale P. Brown and beige fat: development, function and therapeutic
929 potential. *Nature medicine*. 2013;19(10):1252-63.
- 930 28. Zhou Z, Yon Toh S, Chen Z, Guo K, Ng CP, Ponniah S, et al. Cidea-deficient mice have
931 lean phenotype and are resistant to obesity. *Nat Genet*. 2003;35(1):49-56.
- 932 29. Fei W, Shui G, Zhang Y, Krahmer N, Ferguson C, Kapterian TS, et al. A role for
933 phosphatidic acid in the formation of "supersized" lipid droplets. *PLoS Genet*.
934 2011;7(7):e1002201.
- 935 30. Wang H, Zhang J, Qiu W, Han GS, Carman GM, Adeli K. Lipin-1gamma isoform is a novel
936 lipid droplet-associated protein highly expressed in the brain. *FEBS Lett*. 2011;585(12):1979-
937 84.
- 938 31. Marrink SJ, Risselada HJ, Yefimov S, Tieleman DP, de Vries AH. The MARTINI force field:
939 coarse grained model for biomolecular simulations. *The journal of physical chemistry B*.
940 2007;111(27):7812-24.
- 941 32. Mohammadyani D, Tyurin VA, O'Brien M, Sadovsky Y, Gabrilovich DI, Klein-
942 Seetharaman J, et al. Molecular speciation and dynamics of oxidized triacylglycerols in lipid
943 droplets: Mass spectrometry and coarse-grained simulations. *Free radical biology & medicine*.
944 2014;76:53-60.
- 945 33. Rubio-Cabezas O, Puri V, Murano I, Saudek V, Semple RK, Dash S, et al. Partial
946 lipodystrophy and insulin resistant diabetes in a patient with a homozygous nonsense
947 mutation in CIDEA. *EMBO Mol Med*. 2009;1(5):280-7.
- 948 34. Henry SA, Kohlwein SD, Carman GM. Metabolism and regulation of glycerolipids in the
949 yeast *Saccharomyces cerevisiae*. *Genetics*. 2012;190(2):317-49.
- 950 35. Wu C, Zhang Y, Sun Z, Li P. Molecular evolution of Cide family proteins: novel domain
951 formation in early vertebrates and the subsequent divergence. *BMC Evol Biol*. 2008;8:159.
- 952 36. Rose K, Rudge SA, Frohman MA, Morris AJ, Engebrecht J. Phospholipase D signaling is
953 essential for meiosis. *Proc Natl Acad Sci U S A*. 1995;92(26):12151-5.
- 954 37. Choi HS, Su WM, Morgan JM, Han GS, Xu Z, Karanasios E, et al. Phosphorylation of
955 phosphatidate phosphatase regulates its membrane association and physiological functions in
956 *Saccharomyces cerevisiae*: identification of SER(602), THR(723), AND SER(744) as the sites
957 phosphorylated by CDC28 (CDK1)-encoded cyclin-dependent kinase. *J Biol Chem*.
958 2010;286(2):1486-98.
- 959 38. Choi HS, Su WM, Han GS, Plote D, Xu Z, Carman GM. Pho85p-Pho80p phosphorylation
960 of yeast Pah1p phosphatidate phosphatase regulates its activity, location, abundance, and
961 function in lipid metabolism. *J Biol Chem*. 2012;287(14):11290-301.
- 962 39. Han GS, O'Hara L, Carman GM, Siniosoglou S. An unconventional diacylglycerol kinase
963 that regulates phospholipid synthesis and nuclear membrane growth. *J Biol Chem*.
964 2008;283(29):20433-42.

965 40. Fakas S, Konstantinou C, Carman GM. DGK1-encoded diacylglycerol kinase activity is
966 required for phospholipid synthesis during growth resumption from stationary phase in
967 *Saccharomyces cerevisiae*. *J Biol Chem*. 2010;286(2):1464-74.

968 41. Santos-Rosa H, Leung J, Grimsey N, Peak-Chew S, Siniossoglou S. The yeast lipin Smp2
969 couples phospholipid biosynthesis to nuclear membrane growth. *EMBO J*. 2005;24(11):1931-
970 41.

971 42. Adeyo O, Horn PJ, Lee S, Binns DD, Chandrabhas A, Chapman KD, et al. The yeast lipin
972 orthologue Pah1p is important for biogenesis of lipid droplets. *J Cell Biol*. 2011;192(6):1043-55.

973 43. Fakas S, Qiu Y, Dixon JL, Han GS, Ruggles KV, Garbarino J, et al. Phosphatidate
974 phosphatase activity plays key role in protection against fatty acid-induced toxicity in yeast. *J*
975 *Biol Chem*. 2011;286(33):29074-85.

976 44. Sandager L, Gustavsson MH, Stahl U, Dahlqvist A, Wiberg E, Banas A, et al. Storage lipid
977 synthesis is non-essential in yeast. *J Biol Chem*. 2002;277(8):6478-82.

978 45. Han GS, Carman GM. Characterization of the human LPIN1-encoded phosphatidate
979 phosphatase isoforms. *J Biol Chem*. 2010;285(19):14628-38.

980 46. Rosell M, Kaforou M, Frontini A, Okolo A, Chan YW, Nikolopoulou E, et al. Brown and
981 white adipose tissues: intrinsic differences in gene expression and response to cold exposure in
982 mice. *Am J Physiol Endocrinol Metab*. 2014;306(8):E945-64.

983 47. Hallberg M, Morganstein DL, Kiskinis E, Shah K, Kralli A, Dilworth SM, et al. A functional
984 interaction between RIP140 and PGC-1 α regulates the expression of the lipid droplet
985 protein CIDEA. *Mol Cell Biol*. 2008;28(22):6785-95.

986 48. Risselada HJ, Grubmüller H. How SNARE molecules mediate membrane fusion: recent
987 insights from molecular simulations. *Curr Opin Struct Biol*. 2012;22(2):187-96.

988 49. Gubern A, Casas J, Barcelo-Torns M, Barneda D, de la Rosa X, Masgrau R, et al. Group
989 IVA phospholipase A2 is necessary for the biogenesis of lipid droplets. *J Biol Chem*.
990 2008;283(41):27369-82.

991 50. Andersson L, Bostrom P, Ericson J, Rutberg M, Magnusson B, Marchesan D, et al. PLD1
992 and ERK2 regulate cytosolic lipid droplet formation. *J Cell Sci*. 2006;119(Pt 11):2246-57.

993 51. Kooijman EE, Chupin V, Fuller NL, Kozlov MM, de Kruijff B, Burger KN, et al.
994 Spontaneous curvature of phosphatidic acid and lysophosphatidic acid. *Biochemistry*.
995 2005;44(6):2097-102.

996 52. Arisawa K, Ichi I, Yasukawa Y, Sone Y, Fujiwara Y. Changes in the phospholipid fatty acid
997 composition of the lipid droplet during the differentiation of 3T3-L1 adipocytes. *J Biochem*.
998 2013.

999 53. Hörl G, Wagner A, Cole LK, Malli R, Reicher H, Kotzbeck P, et al. Sequential synthesis
1000 and methylation of phosphatidylethanolamine promote lipid droplet biosynthesis and stability
1001 in tissue culture and in vivo. *J Biol Chem*. 2011;286(19):17338-50.

1002 54. Yu J, Zhang S, Cui L, Wang W, Na H, Zhu X, et al. Lipid droplet remodeling and
1003 interaction with mitochondria in mouse brown adipose tissue during cold treatment.
1004 *Biochimica et biophysica acta*. 2015;1853(5):918-28.

1005 55. Mottillo EP, Balasubramanian P, Lee YH, Weng C, Kershaw EE, Granneman JG. Coupling
1006 of lipolysis and de novo lipogenesis in brown, beige, and white adipose tissues during chronic
1007 β 3-adrenergic receptor activation. *Journal of lipid research*. 2014;55(11):2276-86.

1008 56. Bertin R. Glycerokinase activity and lipolysis regulation in brown adipose tissue of cold
1009 acclimated rats. *Biochimie*. 1976;58(4):431-4.

1010 57. Bertin R, Andriamihaja M, Portet R. Glycerokinase activity in brown and white adipose
1011 tissues of cold-adapted obese Zucker rats. *Biochimie*. 1984;66(7-8):569-72.

1012 58. Portet R, Laury MC, Bertin R, Senault C, Hluszko MT, Chevillard L, et al. Hormonal
1013 stimulation of substrate utilization in brown adipose tissue of cold acclimated rats.
1014 *Proceedings of the Society for Experimental Biology and Medicine Society for Experimental*
1015 *Biology and Medicine (New York, NY)*. 1974;147(3):807-12.

1016 59. Kiskinis E, Chatzeli L, Curry E, Kaforou M, Frontini A, Cinti S, et al. RIP140 represses the
 1017 "brown-in-white" adipocyte program including a futile cycle of triacylglycerol breakdown and
 1018 synthesis. *Molecular endocrinology* (Baltimore, Md). 2014;28(3):344-56.
 1019 60. Whittle A, Relat-Pardo J, Vidal-Puig A. Pharmacological strategies for targeting BAT
 1020 thermogenesis. *Trends Pharmacol Sci*. 2013;34(6):347-55.
 1021 61. Krahmer N, Farese RV, Jr., Walther TC. Balancing the fat: lipid droplets and human
 1022 disease. *EMBO Mol Med*. 2013;5(7):973-83.
 1023 62. Li H, Song Y, Li F, Zhang L, Gu Y, Jiang L, et al. Identification of lipid droplet-associated
 1024 proteins in the formation of macrophage-derived foam cells using microarrays. *Int J Mol Med*.
 1025 2010;26(2):231-9.
 1026 63. Zhou L, Xu L, Ye J, Li D, Wang W, Li X, et al. Cidea promotes hepatic steatosis by sensing
 1027 dietary fatty acids. *Hepatology*. 2012;56(1):95-107.
 1028 64. Matsusue K, Kusakabe T, Noguchi T, Takiguchi S, Suzuki T, Yamano S, et al. Hepatic
 1029 steatosis in leptin-deficient mice is promoted by the PPARgamma target gene Fsp27. *Cell*
 1030 *Metab*. 2008;7(4):302-11.
 1031 65. Arnold K, Bordoli L, Kopp J, Schwede T. The SWISS-MODEL workspace: a web-based
 1032 environment for protein structure homology modelling. *Bioinformatics*. 2006;22(2):195-201.
 1033 66. Maupetit J, Derreumaux P, Tuffery P. PEP-FOLD: an online resource for de novo
 1034 peptide structure prediction. *Nucleic Acids Res*. 2009;37(Web Server issue):W498-503.
 1035 67. Trott O, Olson AJ. AutoDock Vina: improving the speed and accuracy of docking with a
 1036 new scoring function, efficient optimization, and multithreading. *J Comput Chem*.
 1037 2009;31(2):455-61.
 1038 68. Monticelli L, Kandasamy SK, Periole X, Larson RG, Tieleman DP, Marrink SJ. The
 1039 MARTINI Coarse-Grained Force Field: Extension to Proteins. *J Chem Theory and Comput*.
 1040 2008;4(5):819-34.
 1041 69. Berendsen HJC, Postma JPM, van Gunsteren WF, DiNola A, R. HJ. Molecular dynamics
 1042 with coupling to an external bath.
 1043 *Journal of Chemical Physics*. 1984;81(8):3684-90.
 1044 70. Humphrey W, Dalke A, Schulten K. VMD: visual molecular dynamics. *J Mol Graph*.
 1045 1996;14(1):33-8, 27-8.
 1046 71. Van Der Spoel D, Lindahl E, Hess B, Groenhof G, Mark AE, Berendsen HJ. GROMACS:
 1047 fast, flexible, and free. *Journal of computational chemistry*. 2005;26(16):1701-18.
 1048 72. Manifava M, Thuring JW, Lim ZY, Packman L, Holmes AB, Ktistakis NT. Differential
 1049 binding of traffic-related proteins to phosphatidic acid- or phosphatidylinositol (4,5)-
 1050 bisphosphate-coupled affinity reagents. *J Biol Chem*. 2001;276(12):8987-94.
 1051 73. Brachmann CB, Davies A, Cost GJ, Caputo E, Li J, Hieter P, et al. Designer deletion
 1052 strains derived from *Saccharomyces cerevisiae* S288C: a useful set of strains and plasmids for
 1053 PCR-mediated gene disruption and other applications. *Yeast*. 1998;14(2):115-32.
 1054 74. Carpenter AE, Jones TR, Lamprecht MR, Clarke C, Kang IH, Friman O, et al. CellProfiler:
 1055 image analysis software for identifying and quantifying cell phenotypes. *Genome Biol*.
 1056 2006;7(10):R100.
 1057 75. Gaspar ML, Aregullin MA, Jesch SA, Henry SA. Inositol induces a profound alteration in
 1058 the pattern and rate of synthesis and turnover of membrane lipids in *Saccharomyces*
 1059 *cerevisiae*. *J Biol Chem*. 2006;281(32):22773-85.

1060

Figure 1

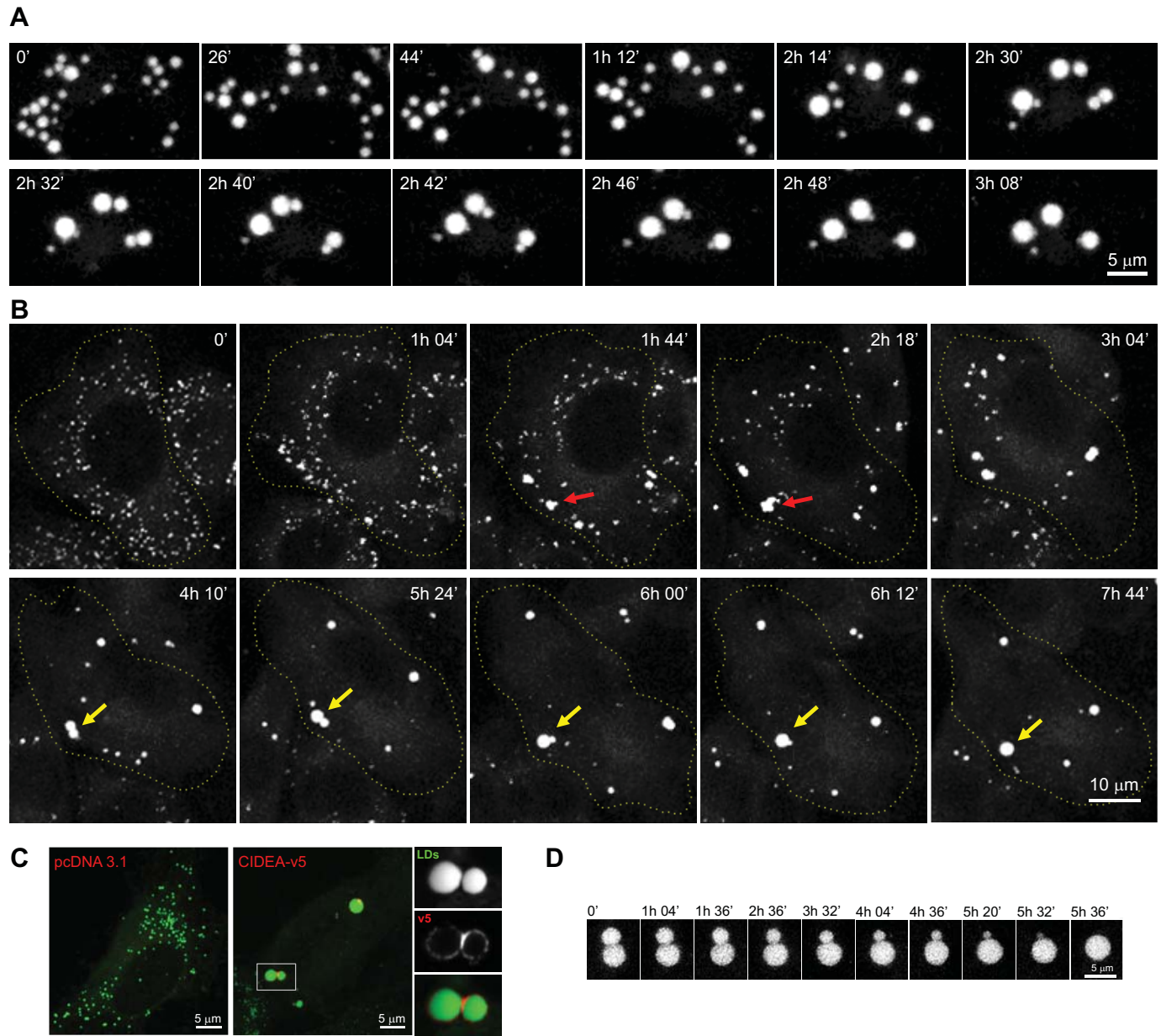
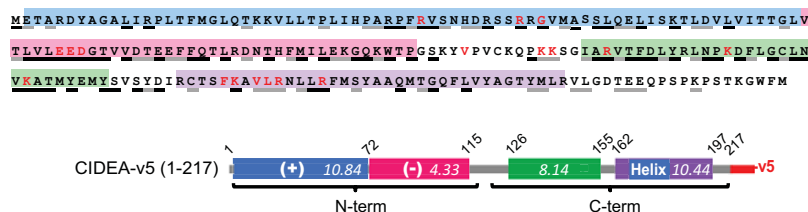
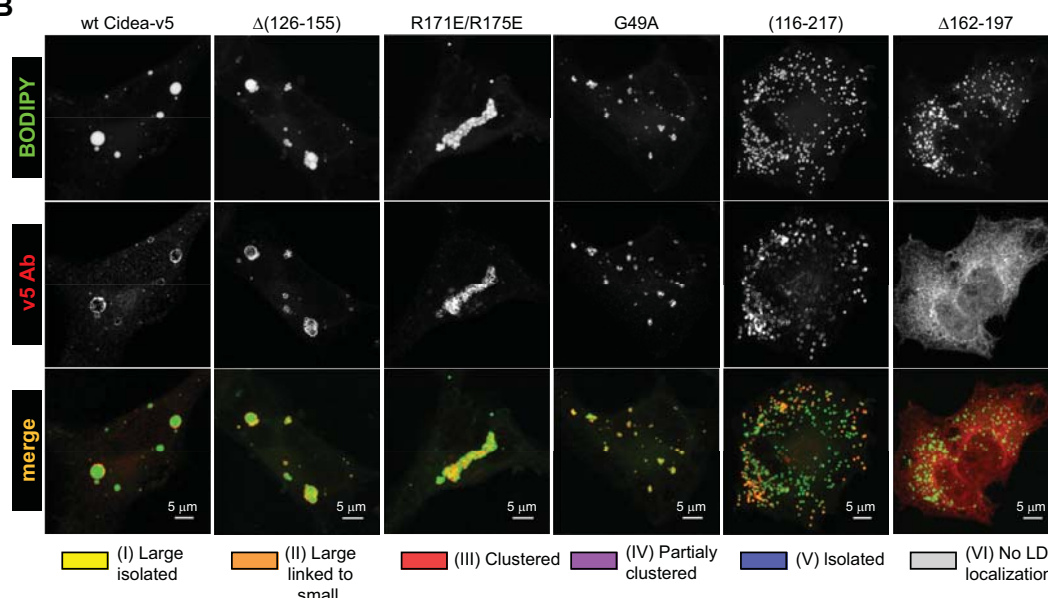


Figure 2

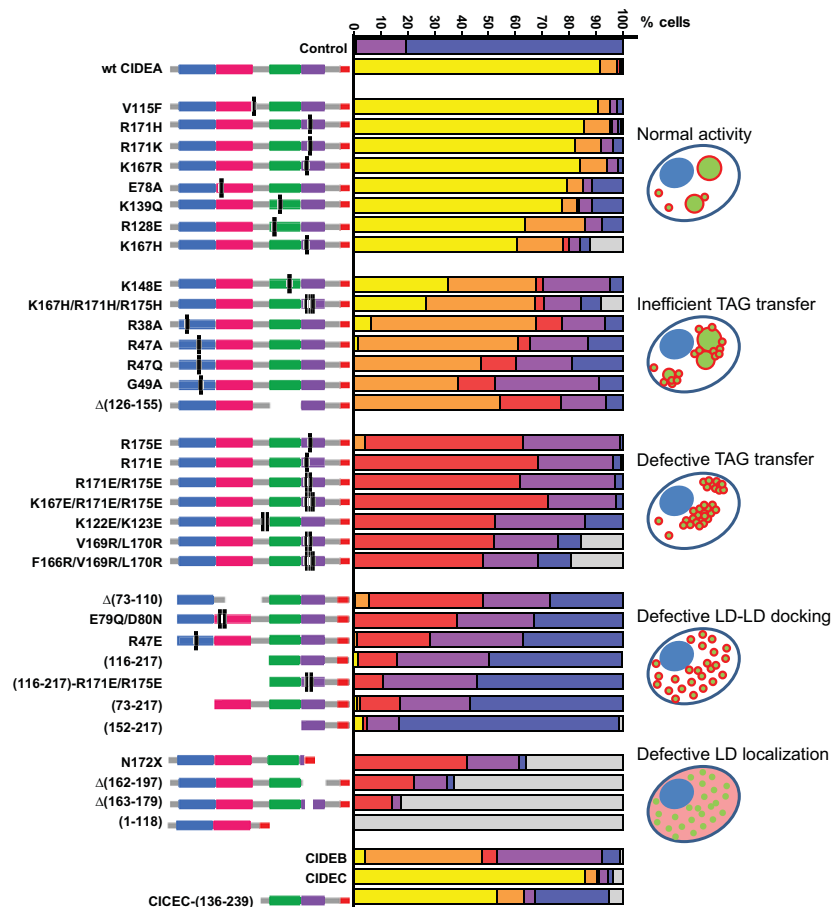
A



B



C



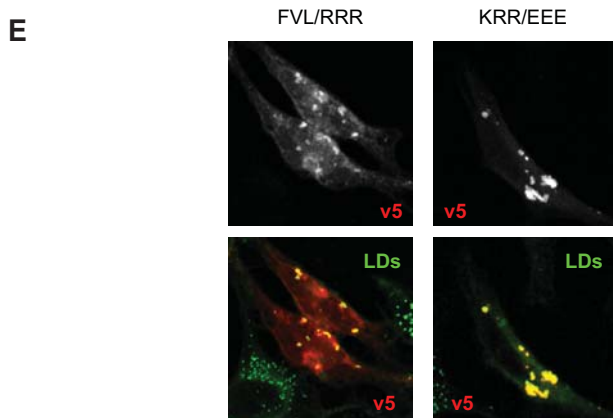
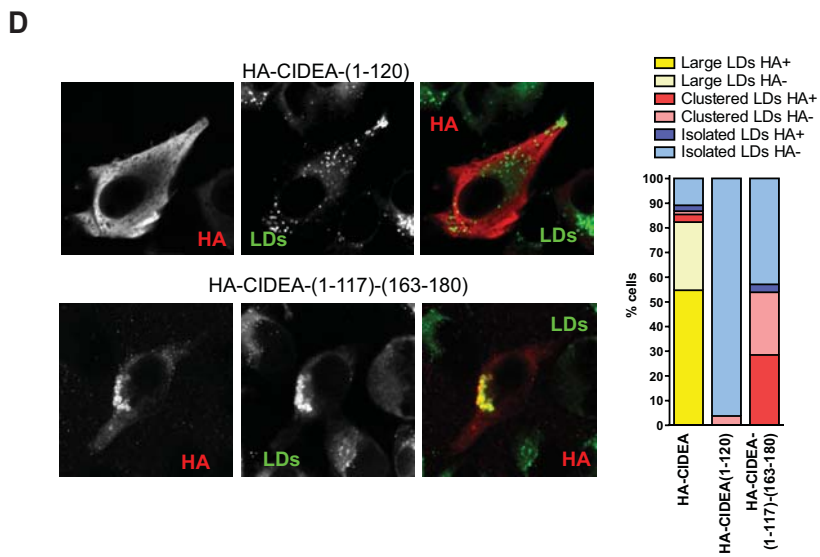
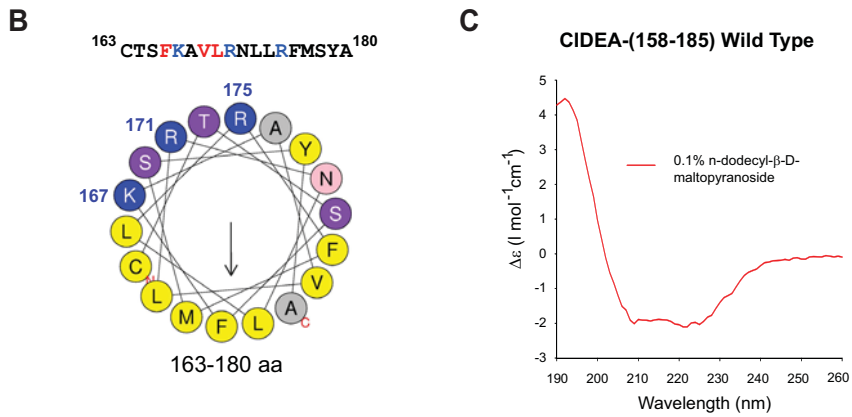
[illegible]

Figure 4

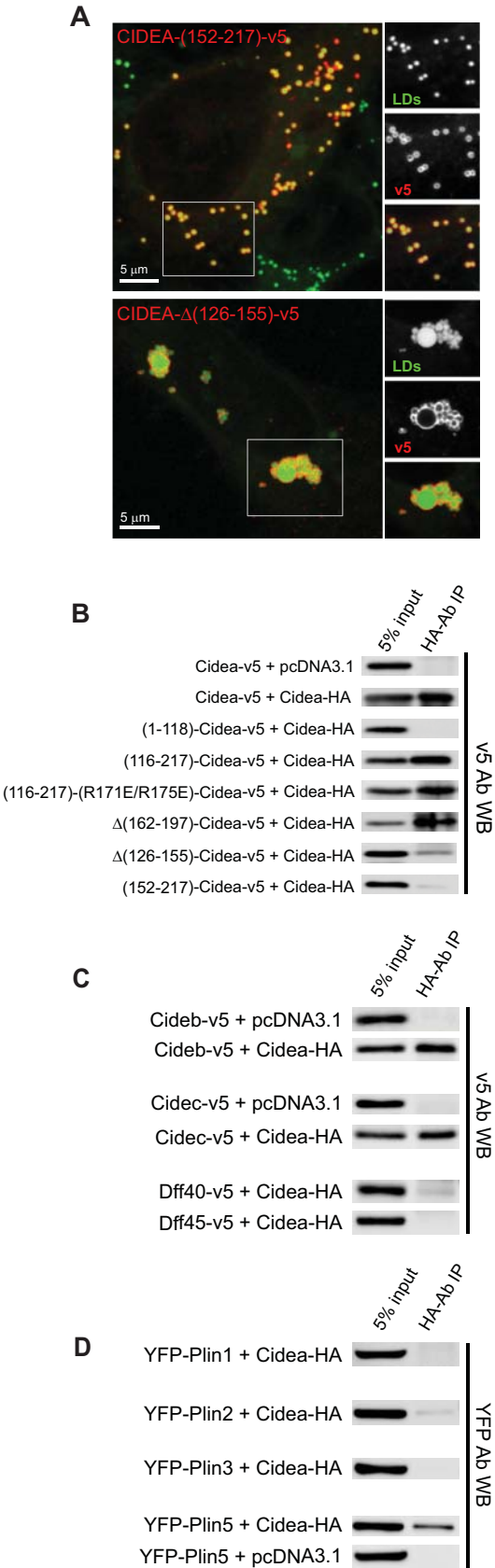


Figure 5

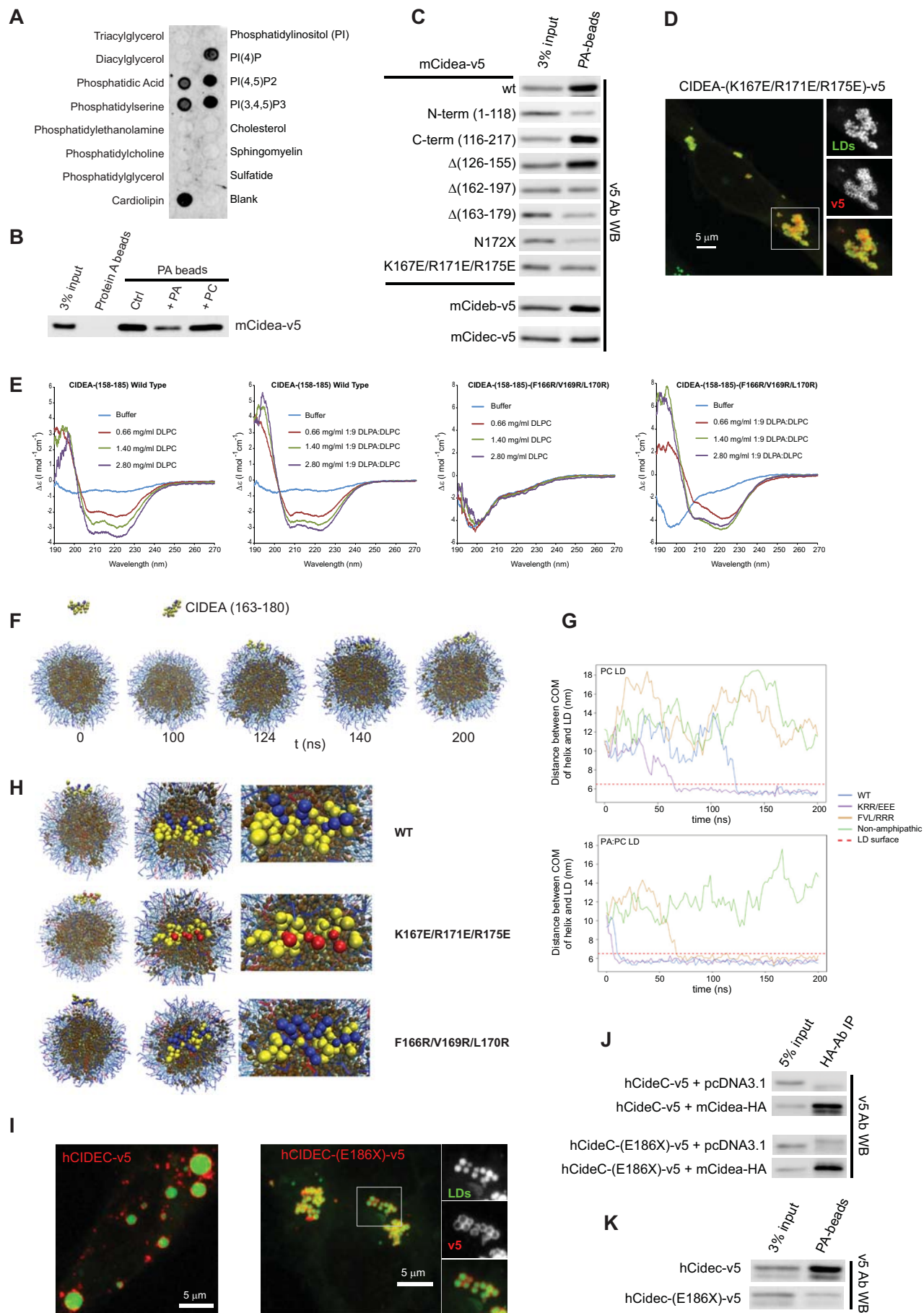


Figure 6

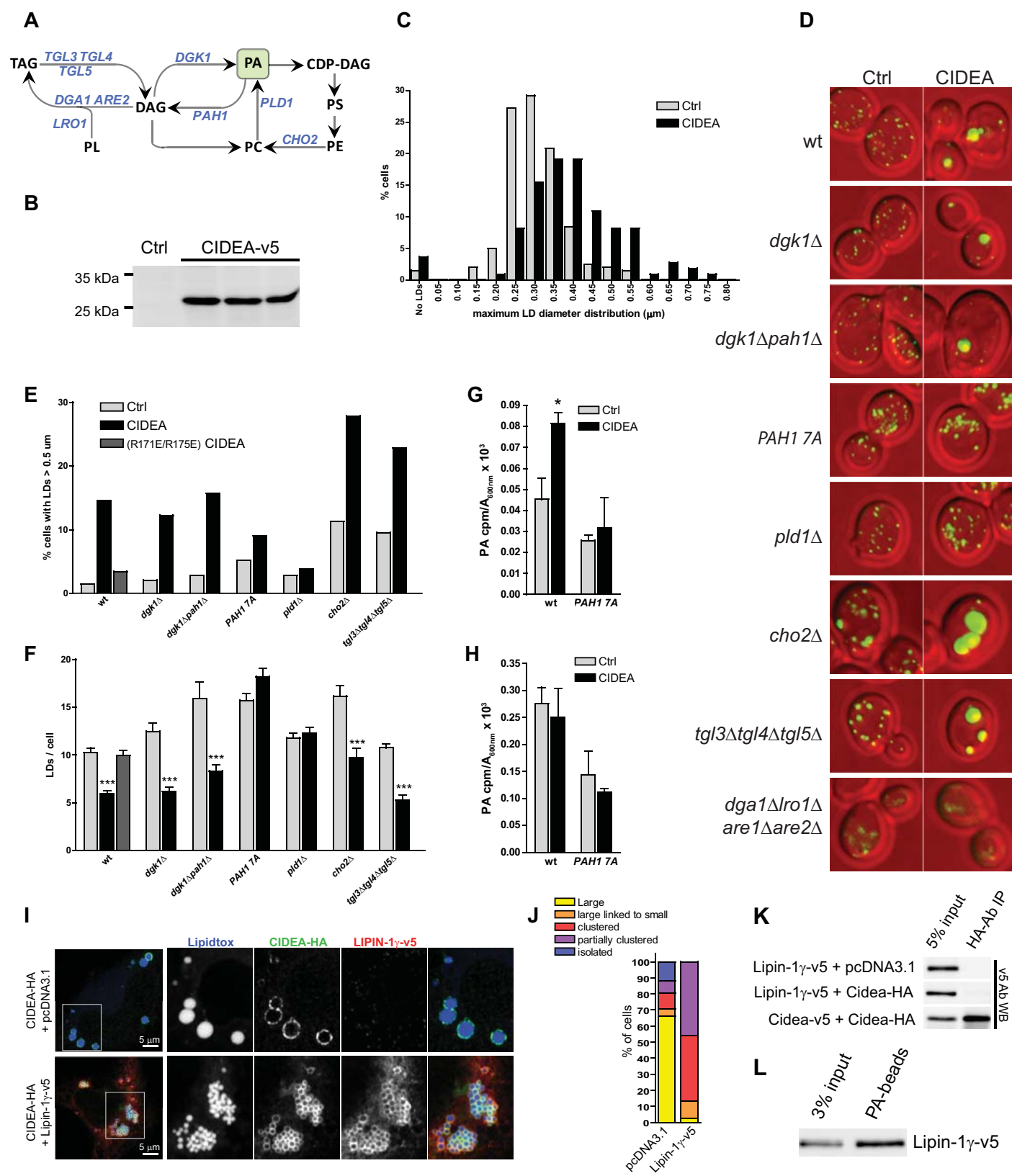
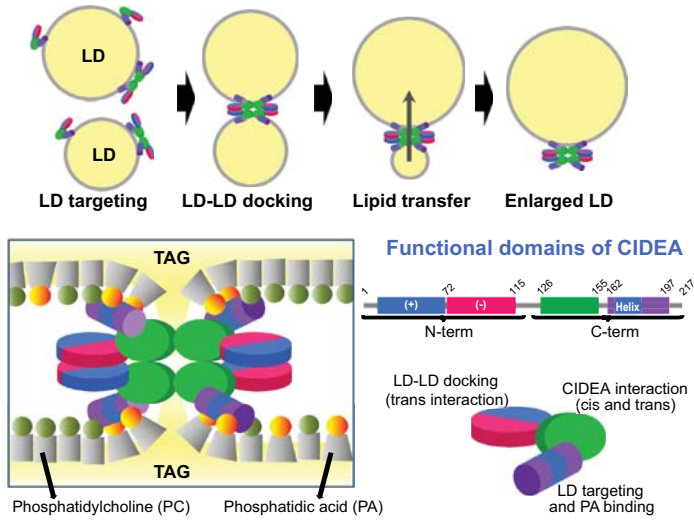


Figure 7

A



B

